Final Technical Report

for

United States Department of Energy
Energy Efficiency and Renewable Energy Department
Award Number: DE-EE0008672

Project Title: Highly-Efficient Microemulsion-Based Absorption Chillers for HVAC Application

Principal Investigator (PI):

Professor Bao Yang
University of Maryland
College Park, MD 20742

Submitted by:
Professor Bao Yang
University of Maryland
College Park, MD 20742

Date: November 9, 2023

ACKNOWLEDGEMENT:

This material is based upon work supported by the U.S. Department of Energy's Office of Energy Efficiency and Renewable Energy (EERE) under the Building Technologies Office (BTO) Award Number DE-EE0008672.

DISCLAIMER:

This report was prepared as an account of work sponsored by an agency of the United States Government. Neither the United States Government nor any agency thereof, nor any of their employees, makes any warranty, express or implied, or assumes any legal liability or responsibility for the accuracy, completeness, or usefulness of any information, apparatus, product, or process disclosed, or represents that its use would not infringe privately owned rights. Reference herein to any specific commercial product, process, or service by trade name, trademark, manufacturer, or otherwise does not necessarily constitute or imply its endorsement, recommendation, or favoring by the United States Government or any agency thereof. The views and opinions of authors expressed herein do not necessarily state or reflect those of the United States Government or any agency thereof.

1. Executive Summary

Air conditioning is a necessity to achieve a comfortable, habitable home or office for many places in US. However, vapor compression air conditioners are largely made with chlorofluorocarbon refrigerants, or CFCs, which create problems for a world grappling with climate change. In addition, vapor compression air conditioners are driven by electricity. Cooling and heating represent one-third of building electrical energy consumption in US.

An absorption chiller is different to vapor compression chillers or air conditioners because it doesn't use conventional refrigerants, like CFC. Instead, they may use water as the refrigerant which is mixed with safe and nontoxic absorbents. More importantly, the absorption chiller can be driven by low-grade heat to produce cooling. However, due mainly to low efficiency, the traditional absorption chillers are limited to niche applications, such as water chiller for air-conditioning in commercial buildings where heat source is available. There is a sizeable global market for the absorption chiller if their efficiency could increase and reach the efficiency of vapor compression air conditioners.

The research performed in this project advanced the understanding of absorption cooling technology and its application in HVAC. Various technologies were explored to improve the performance of the desorber and absorber components in the absorption chillers. The important results achieved in this project are discussed below:

- 1). The reliability of the microemulsion absorbent was tested under thermal cycling. In this accelerated testing, the acceleration factor resulting from the temperature cycle test was about 14.5. The lifetime of the microemulsion absorbent was found to be around 16 years in this test.
- 2). An electrostatic-coalescence desorber was developed, which was an important component of the absorption chiller. Modeling analysis was conducted, in which the dipole-dipole force and dielectrophoresis force were considered to be the main driving forces to cause the droplet coalescence. The electrostatic-coalescence desorber was manufactured and tested. It was found that the desorption time with the assistance of the electrostatic filed could be reduced by more than 10 times compared to the desorption process without the electrostatic field. The strategy to scale up the electrostatic-coalescence desorber was also investigated. The electrostatic separation technology developed in project would be also useful in removing water from oil in petroleum-related industries.
- 3). An absorber using spray nozzles was developed to improve the vapor absorption rate in the microemulsion absorbent, in which diffusion coefficient of refrigerant water was about 30 times less than the value in lithium bromide/water. Theoretical modeling was performed, and it was found that the microemulsion droplet size impacted the absorption rate significantly. Different atomizing spray nozzles were tested for maximization of the absorption rate. The strategy to scale up the absorber capacity was also investigated.
- 4). A chiller configuration using the microemulsions as absorbent was developed, which consisted mainly of a desorber, an absorber, and an evaporator. A prototype absorption chiller was manufactured and analyzed. Unlike the tradition absorption chillers, the condenser was no longer needed in this chiller system. The refrigerant water was desorbed as liquid without vaporization or boiling in the desorber.

These research results demonstrated the feasibility and difficulties of developing a new generation of absorption chillers utilizing the microemulsion absorbents that have the potential to significantly improve the chiller performance.

Table of Contents

1.	Execu	ıtive	Summary	ii
Tal	ole of C	Conte	ents	iii
2.	Backg	grou	nd	1
3.		-	Study of Microemulsion Absorbent	
			ncept of Microemulsion Absorbent	
	3.2	An	alysis of the Microemulsion Stability	5
	3.2.	.1	Temperature Cycling Test	5
	3.2.	.2	Expected Life Of The Microemulsion	7
4.	Devel	lopm	nent of Microemulsion Desorber with Electrostatic Coalescer	10
	4.1	Ele	ectrostatic Separation Analysis	10
	4.1.	.1	Sedimentation of Water Droplets	10
	4.1.	.2	Electric Forces Exerted on Water Droplets	11
	4.1	.3	Uniform electric field or non-uniform electric field	12
	4.1.	.4	Simulation of Electric Field in Desorber	13
	4.2	Ex	periment Results for Desorber	14
	4.2.	.1	Design and Manufacturing of Electrode Array	14
	4.2.	.2	Study on Electrical Waveforms	16
	4.2.	.3	Assembly of Electrostatic Desorber	17
5.	Devel	lopm	nent of Microemulsion Absorber with Atomizing Spray Nozzles	19
	5.1	Mo	odeling On Absorption Process In Microemulsion Droplets	19
	5.2	Nu	meric Simulation on Absorption of Vapor in Microemulsion Droplet	22
	5.3	$\mathbf{E}\mathbf{x}_{1}$	perimental Results for Absorber	26
	5.3	.1	Atomization Techniques For Microemulsion	26
	5.3	.2	Configuration of Integrated Absorber and Evaporator	28
6.	Devel	lopm	nent of prototype microemulsion-based absorption chiller	31
	6.1	Ov	erall System Configuration	31
	6.2	Ex	perimental Results for the Absorption Chiller	32
7.	Concl	lusio	ns and Future Research Recommendation	37
	7.1	Co	nclusions of Experimental and Theoretical Work	37
	7.2	Lir	nitation of the Research and Future Research Recommendation	37
	7.3	Jou	urnal Publications and Conference Products	37
Q	Refer	ence		30

2. Background

An absorption chiller is a cooling machine that uses a heat source (e.g., a fossil-fueled flame, waste heat from factories, or district heating systems) to provide the energy needed to drive the cooling process. Unlike the conventional vapor compression chillers or air conditioners, the absorption chillers do not need electric compressors, which means that they can provide cooling capacity to a facility without contributing to the peak electric demand. Another significant difference with a conventional vapor compression chillers is that the refrigerants primarily used in absorption chillers do not contribute to global warming and ozone depletion. The absorption chiller may use water as the refrigerant which can be mixed with safe and nontoxic absorbents.

In the early years of the 20th century, the absorption chiller using water-ammonia or lithium bromide-water systems was popular and widely used, but after the development of the vapor compression chiller it lost much of its importance because of its low Coefficient of Performance (COP, about one fifth of that of the vapor compression chiller). [1][2] Currently, the absorption chillers are limited to niche applications, such as water chiller for air-conditioning in commercial buildings, where surplus heat is available (e.g., from turbine exhausts or industrial processes), or where electricity is costly or unavailable.

A schematic diagram of a state-of-the-art single effect absorption cycle is shown in Figure 1. An absorption chiller mainly comprises four chambers: absorber, desorber, condenser and evaporator, all connected to each other. The thermodynamic cycle of the conventional absorption chiller consists of a solution loop and refrigerant loop. In the solution loop, the absorbent solution circulates between the desorber and absorber. In the desorber, the amount of heat required for desorption consists of its latent heat of evaporation and heat of mixing with the absorbent, i.e., $Q_d = h_{fg} + \Delta h_{mix}$. The refrigerant loop of the absorption chiller is identical in function to the corresponding components in a vapor-compression cycle. In the refrigerant loop, the refrigerant liquid water exits the desorber and passes through the expansion valve, where it is throttled to a lower pressure. The cooling provided by the evaporator is the latent heat of condensation, $Q_e = h_{fg}$.

There is a theoretical limit on the COP for single-effect absorption or adsorption chillers utilizing conventional absorbents such as lithium bromide and zeolites: [1][2]

$$COP_{limit} = \frac{Q_e}{Q_d + W} = \frac{h_{fg}}{h_{fg} + \Delta h_{mix} + W} < 1$$
 (1)

where W is the auxiliary power consumption, $Q_e = h_{fg}$ is the vaporization heat of the refrigerant in the evaporator for cooling, and the heat of desorption, $Q_d = h_{fg} + \Delta h_{mix}$, which consists of the vaporization heat of the refrigerant, h_{fg} , and the heat of mixing (or heat of dilution) Δh_{mix} . It can be seen that the COP of conventional single-effect absorption or adsorption chillers is always less than 1, since the desorption process requires vaporization of the refrigerant from the sorbent. The COP of practical single-effect sorption cooling systems is typically in the range of 0.5 to 0.7.[3]

In this project, various technologies were explored to enhance the performance of the desorber and absorber components in the absorption chillers that used the microemulsion as absorbent.

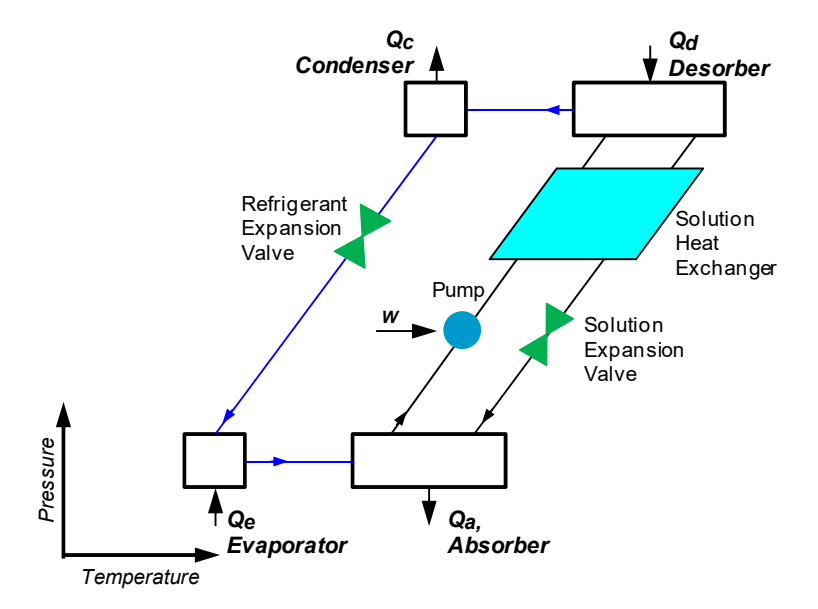


Figure 1: State-of-the-art single-effect absorption cycle schematic.

3. Reliability Study of Microemulsion Absorbent

3.1 Concept of Microemulsion Absorbent

Microemulsion absorbents are a new class of sorption materials invented recently by researchers at the University of Maryland, which consist of inverse micelles of amphiphilic surfactant molecules in apolar oil.[4]-[7] In these microemulsion absorbents, the hydrophobic "tail" of the surfactant molecule is in contact with the surrounding apolar oil, sequestering the hydrophilic "head" group in the micelle center. These hydrophilic "head" groups have strong physicochemical affinity for water molecules, thus leading to absorption of water vapor into the inner surface of the reverse micelles and resulting in the formation of water nanodroplets (see Figure 2).

As temperature increases, the hydrogen bond between the surfactant hydrophilic "head" and water molecules weakens. Consequently, the inverse micelles disassociate in apolar oil while releasing the water nanodroplets. Since the temperature is below the water boiling point, these liquid water droplets will grow by coalescence and eventually settle to the bottom, due to gravity. In this unique desorption process, the water is desorbed as *liquid* without vaporization or boiling, and therefore the heat of desorption $Q_{d,\ conventional}$ is equal of the heat of mixing Δh_{mix} , eliminating the latent heat of vaporization of water h_{fg} . Thus, the heat of desorption in the proposed microemulsion can be many times less than that of all the previously known sorption materials utilized in refrigerator and heat pump applications.

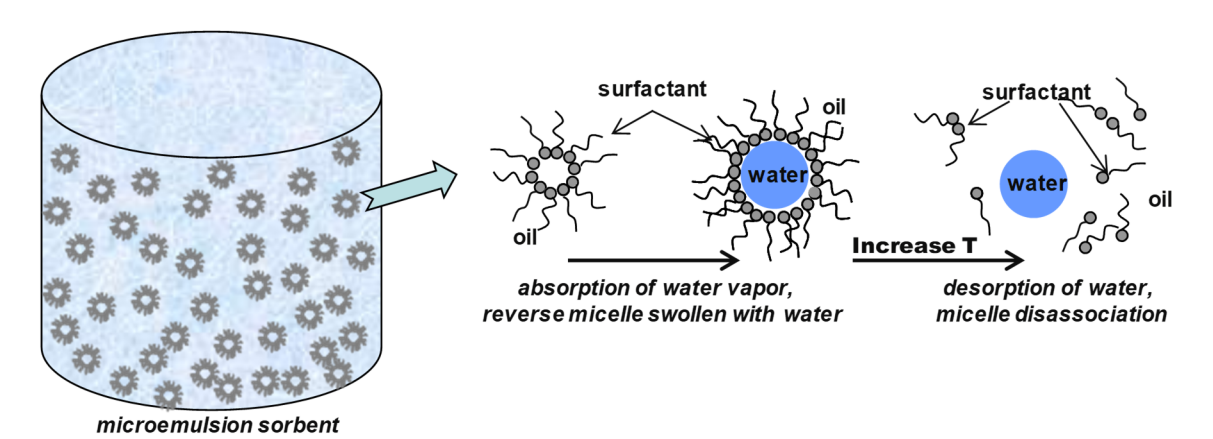


Figure 2: Schematic drawing of the microemulsion absorbent and the inverse micelles of amphiphilic surfactant dispersed within apolar oil. The surfactant micelles absorb vapor during absorption process with associated increase in micelle size. The inverse micelles disassociate at elevated temperatures, and thus the water droplets are desorbed in liquid phase.

The absorption and desorption processes in the microemulsion absorbent is illustrated in Figure 3,

- 1-2: Absorption of water vapor by the microemulsion absorbent until the water concentration increases up to saturation. Heat of absorption Q_a will be released.
- **2-3:** Desorption of water out of the microemulsion absorbent when temperature is increased to a triggering temperature, T_d . Heat of desorption Q_d will be supplied.
- **3-4:** Removal of the desorbed liquid water.
- **4-1:** Regeneration of the microemulsion absorbent by decreasing the temperature.

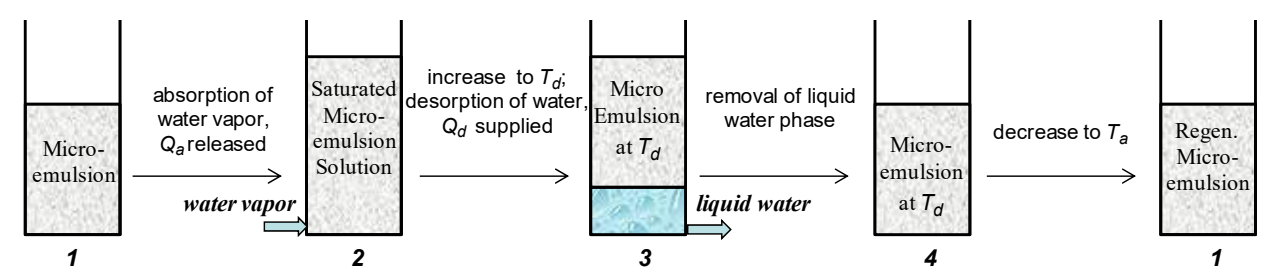
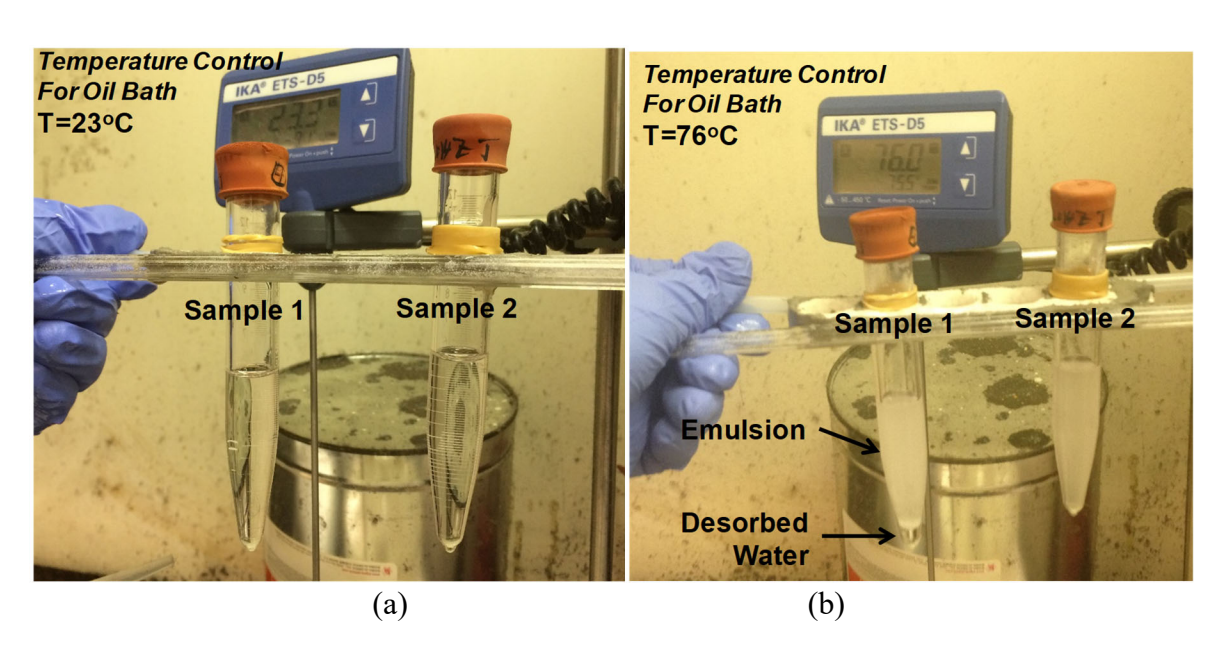


Figure 3: Illustration of water absorption and desorption processes using the microemulsion absorbent.

The desorption of water from the microemulsion absorbent was determined with a temperature-controlled oil bath, as shown in Figure 4a&b. It can be seen that water was separated at the bottom of the microemulsion sample 1, as liquid without vaporization or boiling, when temperature increases to 76°C, which is far below water's boiling point. The desorption process took several hours to complete when the microemulsion temperature was kept at 76°C. Increasing temperature and/or applying electric field could reduce the desorption time to several minutes as discussed in the next chapter. The purity of the desorbed water was determined by measuring the optical absorption spectra of the desorbed water and the water samples with known concentration of surfactant and as can be seen in Figure 4c, the concentration of the impurities in the desorbed water was very small, about 0.6%.



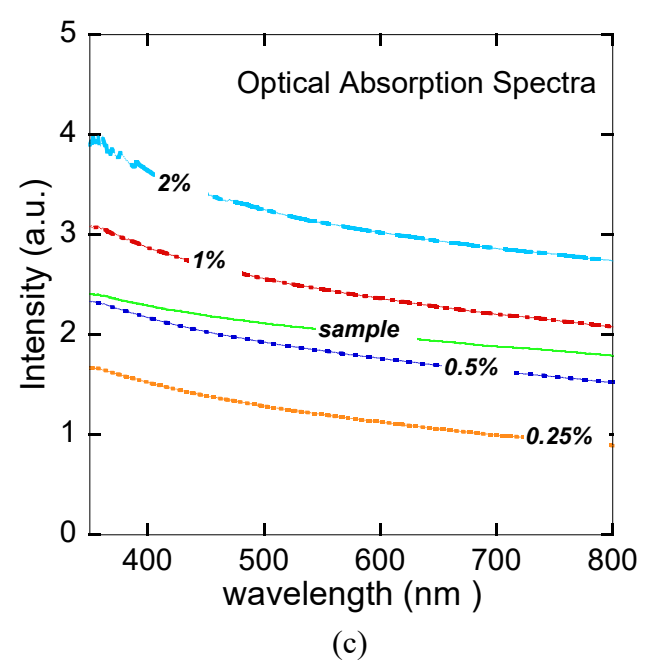


Figure 4: (a) and (b) show the desorption of water from the microemulsion absorbents. (a), Two different microemulsion samples, each containing 5 wt. water, at room temperature. (b), Sample 1 is successful, where water is separated at the bottom when the temperature of the oil bath rises to 76°C. Sample 2 doesn't work. Both microemulsion samples are heated in an oil bath (not shown in the picture) with a temperature controller (IKA ETS-DS). (c) Optical absorption spectra of the desorbed water sample and the water samples containing 2 wt.%, 1 wt.%, 0.5 wt.% and 0.25 wt.% of surfactant. The absorption spectra were measured using a Cary 100 UV-Vis Spectrophotometer.

3.2 Analysis of the Microemulsion Stability

3.2.1 Temperature Cycling Test

The microemulsion absorbent was tested for 70 temperature cycles between 15 °C and 95 °C. The IR spectra of the microemulsion were measured and the change in chemical composition had not been observed during the temperature cycling tests. The detailed results are discussed below.

The microemulsion (about 50 mL) was placed in sealed glass tubes for temperature cycling testing. A temperature-controlled oven was set at 95 °C and served as the hot chamber. A temperature-controlled water bath circulator (isotemp) was set at 15 °C and served as the cold chamber. The microemulsion samples were transferred between these two chambers. Each cycle took about 1 hour in average. A photo of the experimental setup was taken for each temperature cycle. Figure 5 shows the photos of Cycle-1 test and Cycle-70 test, where the chamber temperature and cycle number can be seen.



Figure 5: Photos of the temperature cycling test setup. Top photo: Cycle 1. Bottom photo: Cycle 70.

Infrared (IR) spectroscopy is a simple and reliable technique widely used in both organic and inorganic chemistry, in research and industry.[8][10] IR spectroscopy is often used to identify structures because the functional groups give rise to characteristic bands in terms of both intensity and position (frequency). The positions of these bands are summarized in correlation tables as shown below (see Figure 6).

In this project, the IR spectroscopy was used to identify possible degradation of microemulsions during the temperature-cycling test. IR spectra of the microemulsion samples were measured every 5 cycles, using the Fourier transform infrared (FTIR) spectrometer (Thermo Nicolet NEXUS 670).

The IR spectra of the microemulsion samples before the temperature-cycling test and after the 70^{th} cycle are compared in Figure 7. As shown in these figures, no noticeable differences in these IR spectra are observed during the temperature cycling tests. This indicates that the microemulsions have very good chemical stability.

Type of bond	Wavenumber (cm ⁻¹)	Intensity
C=N	2260-2220	medium
C = C	2260-2100	medium to weak
C=C	1680-1600	medium
C=N	1650-1550	medium
\bigcirc	~1600 and ~1500-1430	strong to weak
c=o	1780-1650	strong
c-o	1250-1050	strong
C-N	1230-1020	medium
O-H (alcohol)	3650-3200	strong, broad
O—H (carboxylic acid)	3300-2500	strong, very broad
N-H	3500-3300	medium, broad
С-Н	3300-2700	medium

Figure 6: List of main IR spectroscopy bands. Wavenumbers listed in cm⁻¹.

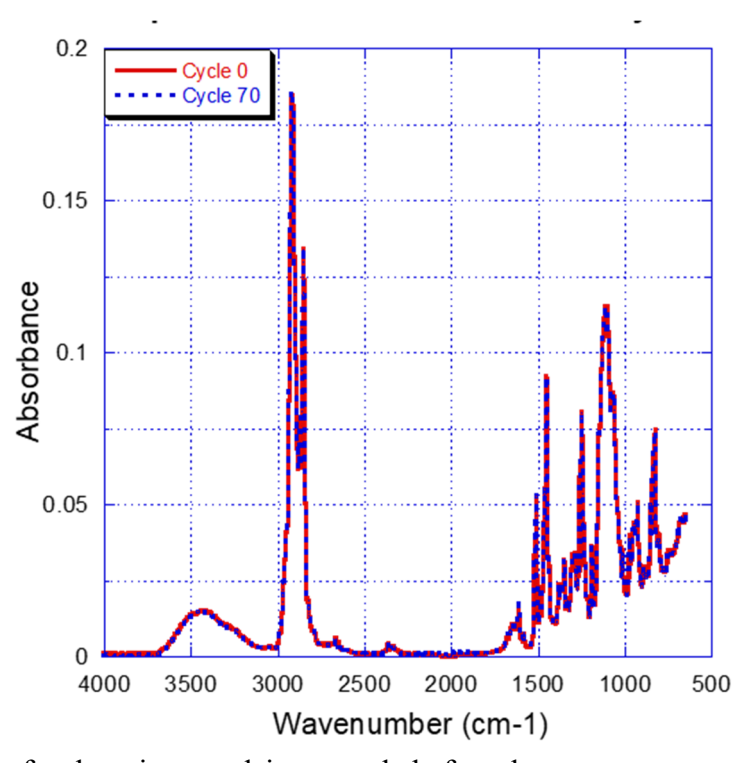


Figure 7: IR spectra for the microemulsion sample before the temperature cycling test, and after 70 cycles.

3.2.2 Expected Life Of The Microemulsion

In the IR spectrum of microemulsion, the two strong peaks were found to be at 2716 cm⁻¹ and 1107 cm⁻¹, which were attributed to the absorption from the -C-H bond and -C-O- bond,

respectively. The IR absorbance was almost linearly depends on the mass concentration of the absorption material, based on Beer–Lambert law.[11] Here, these two IR absorbance peaks were used to estimate the expected life of the microemulsion. Table 1 lists the peak values at 2716 cm⁻¹ and 1107 cm⁻¹ during the temperature cycling tests as well as their average and standard deviation. As seen in this table, the decaying trend during the test was too small to be observed. So the upper bound of the peak value change can be approximated by its standard deviation. Therefore, the decay rate of the absorbance peak after one temperature cycling test is given by,

$$V_{change} = V_0 - V_0 (1 - r)^{70} (2)$$

where V_0 is the initial value of the absorbance peak before the temperature cycling test, V_{change} is the change of the absorbance peak value after 70 cycles, and r is the decay rate for one cycle. It is assumed that the microemulsion absorbent can be in use if the change of the absorbance peak value is less than 50%. Therefore, the lifetime in years under the accelerated conditions is

$$t_{\text{accel}} = Log(0.5)/(24 * 365 * Log(1-r)) \tag{3}$$

The normal operation temperature for the microemulsion absorbents was from 20 °C to 90 °C. The temperature cycling test for the microemulsions was performed between 15 °C and 95 °C. The acceleration factor resulting from the temperature cycle test, AF, is given by the Coffin-Manson equation,

$$AF = (\Delta T_{\text{accel}} / \Delta T_{\text{normal}})^m \tag{4}$$

where $\Delta T_{\rm accel}$ is the temperature difference in accelerated test condition, $\Delta T_{\rm normal}$ is the temperature difference in normal operation condition, m is an exponent constant. The exponent constant m would vary from the test materials and is usually set to be 20 for temperate sensitive-materials like polymer and plastic.[12][13] In this temperature cycling test, the *AF* was calculated to be around 14.5. The lifetime of the microemulsion under normal operation temperature could be calculated by [14]

$$t_{\text{normal}} = AF \cdot t_{\text{accel}},\tag{5}$$

which was found to be around 16 year, as shown in Table 2.

Table 1: Peak values at 2716 cm⁻¹ and 1107 cm⁻¹ and their standard deviation

	Absorbance		
	2716 cm ⁻¹	1107 cm ⁻¹	
Before test	0.185	0.114	
5 th cycle	0.187	0.114	

10 th cycle	0.188	0.114		
15 th cycle	0.186	0.113		
20 th cycle	0.187	0.114		
25 th cycle	0.186	0.113		
30 th cycle	0.188	0.114		
35 th cycle	0.188	0.114		
40 th cycle	0.187	0.114		
45 th cycle	0.186	0.113		
50 th cycle	0.186	0.114		
55 th cycle	0.188	0.115		
60 th cycle	0.186	0.113		
65 th cycle	0.187	0.114		
70 th cycle	0.186	0.114		
Averaged peak value	0.1867	0.1138		
Standard Deviation (STD)	0.0009612	0.0005606		

Table 2: Estimated lifetime of the microemulsion based on IR spectra

Wave number	2716 cm ⁻¹	1107 cm ⁻¹
Standard Deviation (STD)	0.0009612	0.0005606
Decay Rate (r)	0.007441%	0.007042%
$t_{ m accel}$	1.06 years	1.12 years
$t_{ m normal}$ (expected life)	15.36 years	16.24 years

4. **Development of Microemulsion Desorber with Electrostatic Coalescer**

A desorber is a critical component in the microemulsion absorption chiller, in which the refrigerant water is separated from the microemulsion absorbent. It was observed that the water droplets took more than 2 hours to settle down in the microemulsion desorber when under the influence of gravity alone. In this task, numeric simulation and modeling were performed to study the electrostatic field and its effects on the water droplet separation in the desorber. Then, an advanced electrostatic desorber was designed, manufactured, and tested, to accelerate the desorption process.

Electrostatic Separation Analysis 4.1

Sedimentation of Water Droplets 4.1.1

In electric fields, small water droplets move towards each other or collide with each other due to the electrostatic forces, such as dipole-dipole interaction and dielectrophoretic force, acting on them. As a result, the merging and coalescence of those droplets will increase the droplet size and eventually lead to settling and separation of water from the microemulsion.

The balance of the forces acting on a pair of droplets is indicated in Figure 8. Electrostatic and gravitational forces are mainly considered in this analysis. As shown in Figure 8, horizontal electric force (Fel) is created because electrodes are located vertically in our system, while the gravity (F_g) acts vertically to the ground. The velocity of the droplets can be decomposed into horizontal direction V_H and vertical direction V_V. The droplets also experience a flow resistance force (F_v) when moving in microemulsion. The flow resistance force can be decomposed into horizontal (F_{V,H}) and vertical (F_{V,V}) directions.

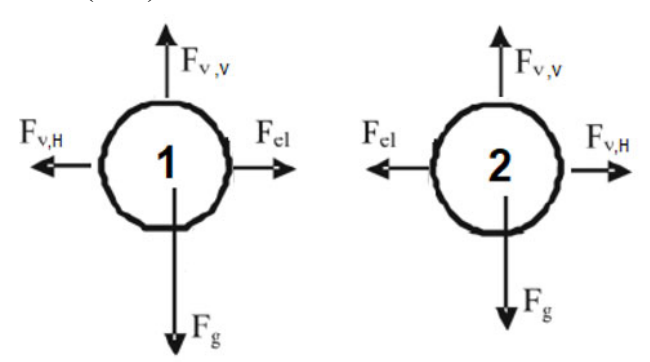


Figure 8. The balance of the forces acting on a pair of droplets when subject to a horizontal electric field.

In the vertical movement, the gravity force (F_g) and the vertical flow resistance force (Fv,v) are considered. The vertical terminal velocity (V_V) can be calculated using sedimentation time (t_V) of the droplet can be obtained using Eq. (7) with a vertical distance h.

$$V_V = \frac{a^2(\rho_W - \rho_O)g}{4.5\mu_O}$$

$$t_V = \frac{4.5\mu_O h}{a^2(\rho_W - \rho_O)g}$$
(6)
(7)

$$t_V = \frac{4.5\mu_0 n}{a^2 (\rho_W - \rho_0)g} \tag{7}$$

The sedimentation time of water droplets can be affected by several factors such as the densities of water and oil $(\rho_w - \rho_o)$, microemulsion viscosity (μ_o) , and radius (a) of the water droplets, as shown in Eq. 7. Figure 9 shows the sedimentation time for water droplets with different radius and different viscosity. It can be seen that the sedimentation time decreases exponentially with increasing droplet size, and it increases linearly with increasing viscosity of the microemulsion. Water droplets have to have large enough falling speed to fall to the bottom of the container. This means that the water droplets have to grow to a large enough size. In addition, reducing the viscosity by increasing the microemulsion temperature will also accelerate the water droplet separation.

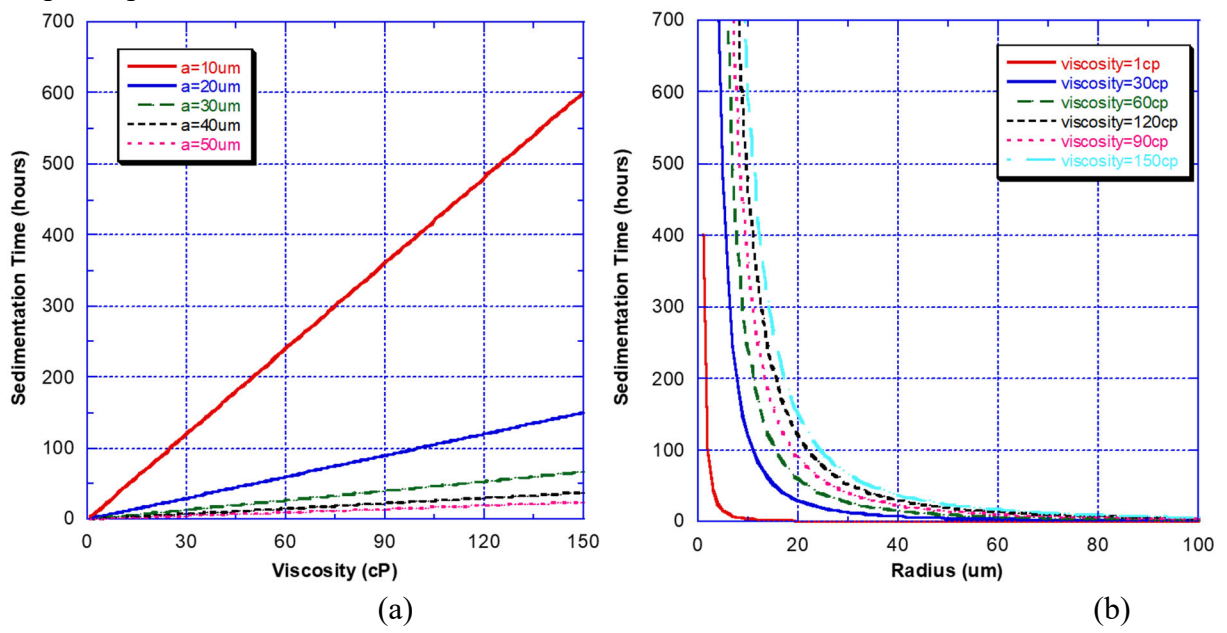


Figure 9: (a) Sedimentation time of water droplets versus viscosity of the microemulsion for different droplet radius. (b) Sedimentation time of water droplets versus radius of water droplets for different viscosity of the microemulsion.

4.1.2 Electric Forces Exerted on Water Droplets

In the desorber developed by the UMD team, the electric field is applied to promote the coalescence of small water droplets in microemulsion. In the separation process, two different electrostatic forces are considered to be the main driving forces: the dipole-dipole force and dielectrophoresis (DEP) force (see Figure 10).

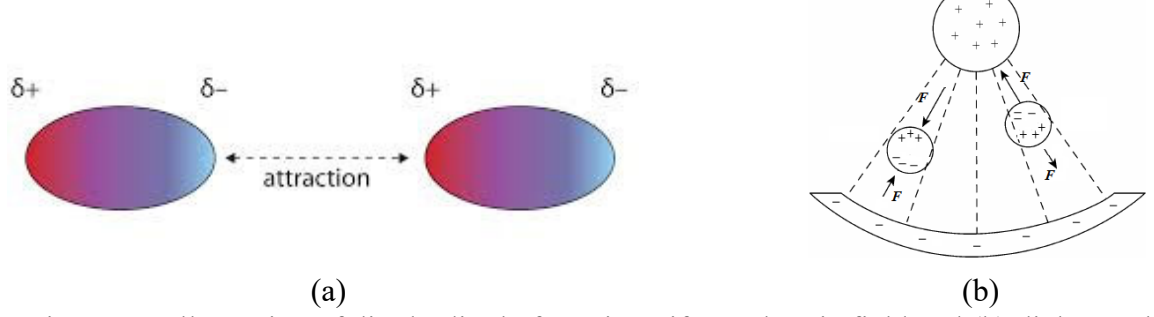


Figure 10: Illustration of dipole-dipole force in uniform electric field and (b) dielectrophoresis (DEP) force in non-uniform electric field.

The dipole-dipole force can be generated both in uniform and non-uniform electric fields. It represents the attractive force between the polarized droplets at the positive end and negative end, which is given by

$$F_{el} = \frac{24\pi\varepsilon E_0^2 a^6}{l^4} \tag{8}$$

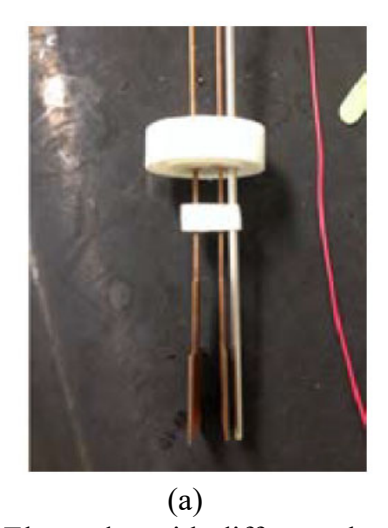
where ε is a permittivity of the medium surrounding oil, E_0 is the strength of the electric field and l is the distance between the droplet centers, and a is the radius of the water droplets. The dielectrophoresis force is exerted on the dielectric water droplets when they are subjected to a non-uniform electric field, which is given by

$$F_{DEP} = 2\pi a^3 \varepsilon_m \frac{\varepsilon_p - \varepsilon_m}{\varepsilon_p + 2\varepsilon_m} \nabla \left| \vec{E} \right|^2. \tag{9}$$

Both uniform and non-uniform electric fields have been tested experimentally in order to determine which electrostatic force is dominant in the separation process. It is found that the non-uniform radial electric field generated by the tube-wire electrodes is much more effective than the uniform electric field to accelerate the water droplet separation. This indicates that the dielectrophoresis force is the dominant electric force exerting on the water droplets in microemulsion. This is because the water droplets are not electrically charged and the microemulsion is essentially an electric insulator. This finding provides us the guideline in the design of the electrodes and electric field; the gradient of the electric field needs to be maximized to increase the collision rate of water droplets in microemulsion.

4.1.3 Uniform electric field or non-uniform electric field

In this test, two different separators, which used flat plates and cylindrical (or wire inside tube) electrodes respectively (see Figure 11), were designed to perform microemulsion separation tests. The flat plate separator was used to create uniform electric fields, while the cylindrical separator is used to provide the non-uniform electric fields. In this test, 1kV of voltage was applied with 50Hz of frequency, and the operating temperature is 90°C. It was found that the radial electric field generated by the tube-wire electrodes can separate out water in the shortest time, less than 1 minute. In comparison, the uniform electric field generated by the parallel plates had little effect on the separation rate of the emulsion, and the separation time was still more than 1 hour. This experiment indicates that dielectrophoresis (DEP) force in the non-uniform electric field is the dominant force.



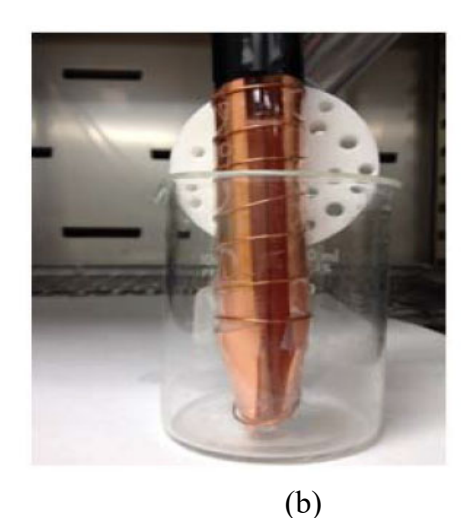


Figure 11: Electrodes with different shapes, such as two parallel plates (a), and wire inside tube (b). The parallel plates can generate uniform electric field while the tube-wire electrodes generate non-uniform, radial electric field.

4.1.4 Simulation of Electric Field in Desorber

The capacity of the electrostatic desorber can be scaled up by using arrays of wire electrodes that can divide a large volume desorber into small unit cells. Each of these unit cells can achieve sufficiently high electric field gradient to accelerate the water separation rate. The magnitude of dielectrophoretic forces acting on the water droplets is proportional to the $\nabla |E|^2$. $\nabla |E|^2$ decreases significantly with the distance from the center electrode. Electric field and its electric field gradient were simulated using the commercial ANSYS software for optimization of the electrode configuration. The design of the electrode configuration was inspired by the honeycomb shape, in which the unit cell was a hexagon. Two arrangements of the ground electrodes were tested first; one used two ground electrodes in one side of the hexagon and the other used three electrodes. Figure 12 shows the electric field map of these three electrode configurations. It can be seen that three wire electrodes would be sufficient to simulate a solid hexagonal electrode (patter 3 in Figure 12). The use of less number of wire electrodes will reduce the difficulty in manufacturing.

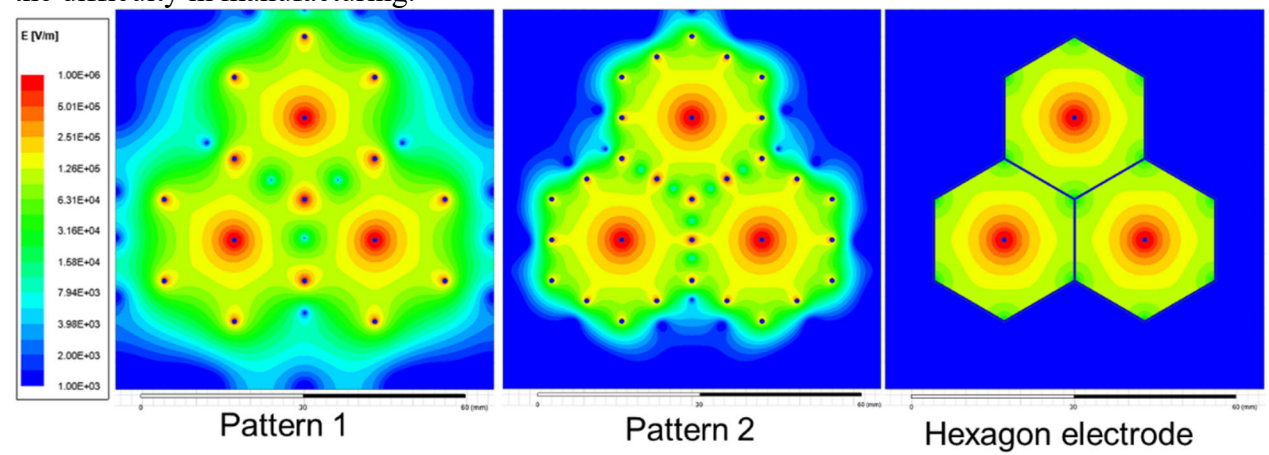


Figure 12: Electric field of three different hexagon type electrode configuration. Pattern 1: two ground wire electrodes in one side. Pattern 2: three ground wire electrodes in one side. Pattern 3: a solid flat plane in one side.

A large area with a strong electric field gradient $\nabla |E|$ can be generated by the repetition of the hexagonal unit cell in different directions. Figure 13 shows the electric field with 4x4 unit cells.

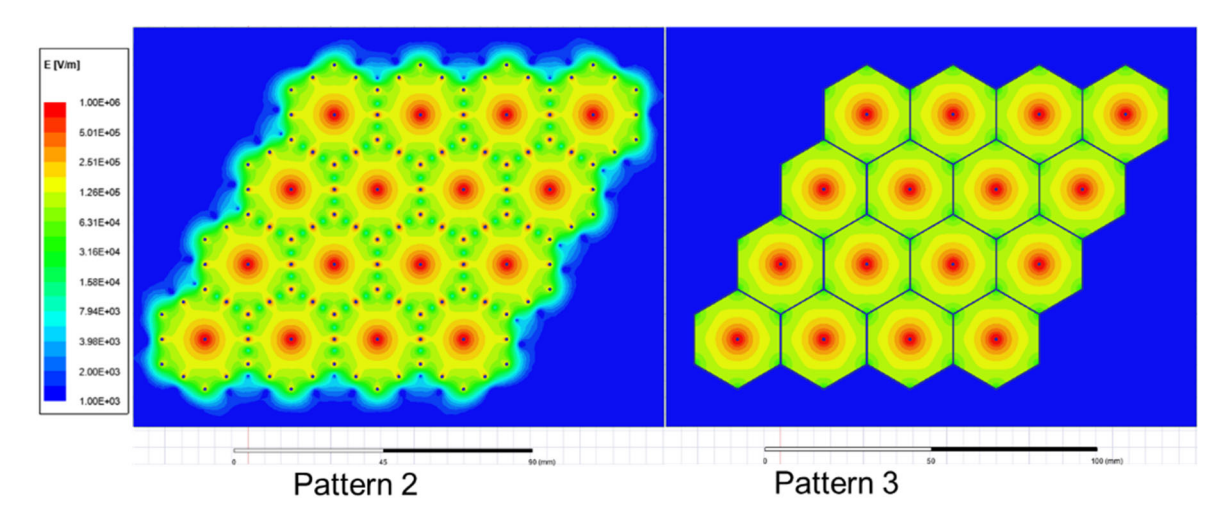


Figure 13: Electric field of 4x4 hexagonal unit cells. Pattern 2: three ground wire electrodes in one side. Pattern 3: a solid flat plane in one side.

4.2 Experiment Results for Desorber

4.2.1 Design and Manufacturing of Electrode Array

Figure 14 shows the configuration of one electrostatic desorber. The electrostatic desorber consisted of a flask, which served as container and was surrounded with copper foil; an electrode base, which was the lid of the flask and also served as the host of wire electrodes; a sealing clamp. The top and bottom view of the electrode base is shown in Figure 14 (b) and (c), respectively. The base was manufactured from PTFE (polytetrafluoroethylene, known as Teflon) using the computer numeric control machine. The hexagon unit cell had a side length of 15mm. There were 13 high voltage electrodes and 66 grounded electrodes. Each high voltage electrode was surrounded by 12 grounded electrodes that form a hexagon.

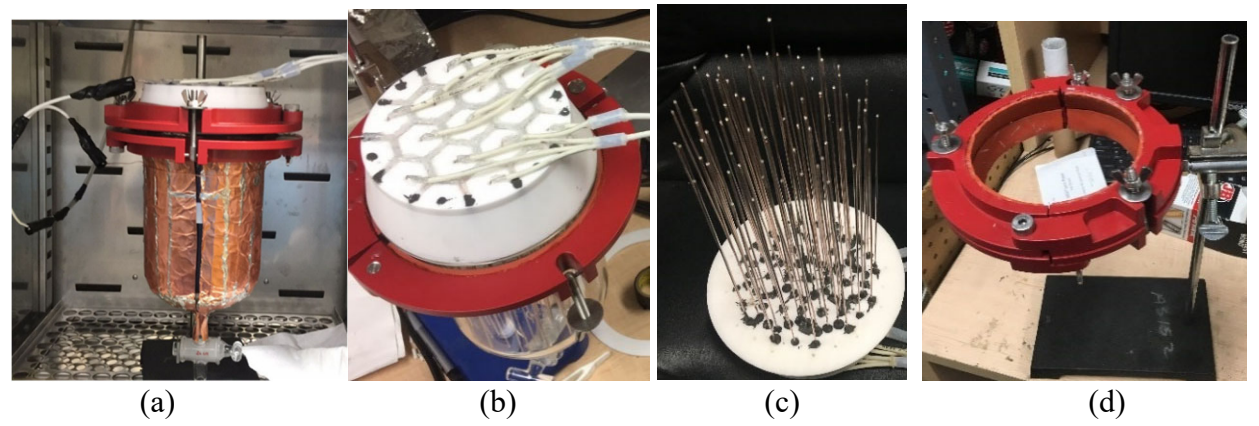


Figure 14. Components of one electrostatic desorber. (a) Flask surrounded with copper foil; (b) top-view of the electrode base; (c) bottom-view of the electrode base; (d) Sealing clamp

Vapor leakage was observed through the epoxy between the electrodes and the PTEF base due to the poor adhesion of the PTEF base. PEEK (Polyether ether ketone) is a semicrystalline thermoplastic with excellent mechanical and chemical resistance properties, and it was used to replace PTEF to figure out vapor leakage issue in the desorber. Numeric simulation was conducted to improve the performance of the electrostatic desorber (see Figure 15 and Figure 16). The side length of the hexagon unit cell was decreased from 15mm in the first generation to 9mm in the fourth generation to increase the electric field gradient. Correspondingly, the number of small unit cells has been increased from 19 to 37 in the desorber tube.

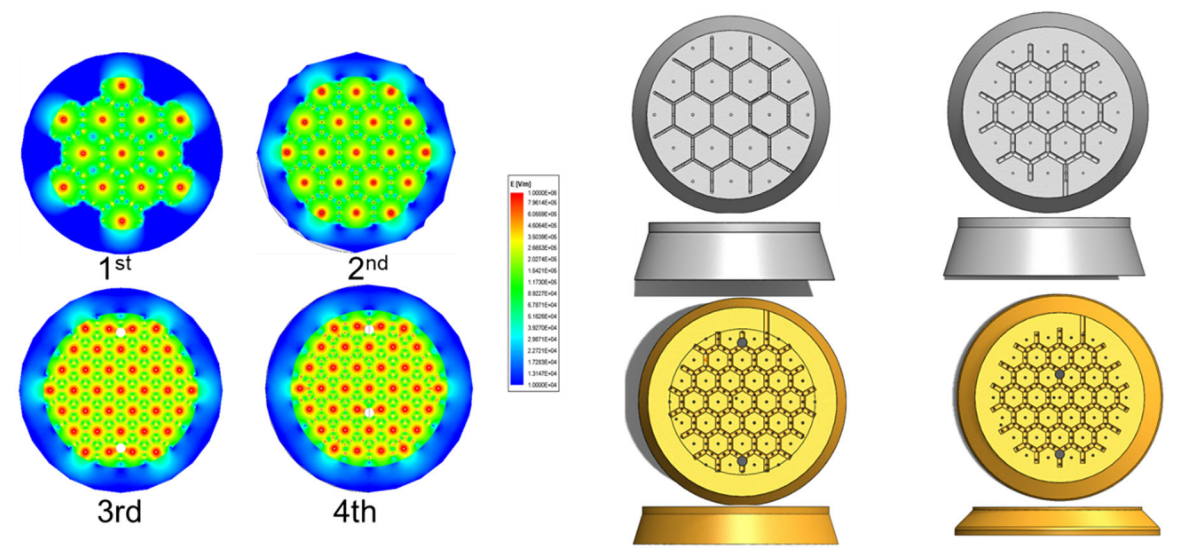


Figure 15: (Left) Electric field in the cross-section for all four generations of desorbers. (Right) CAD drawing of the electrode bases.

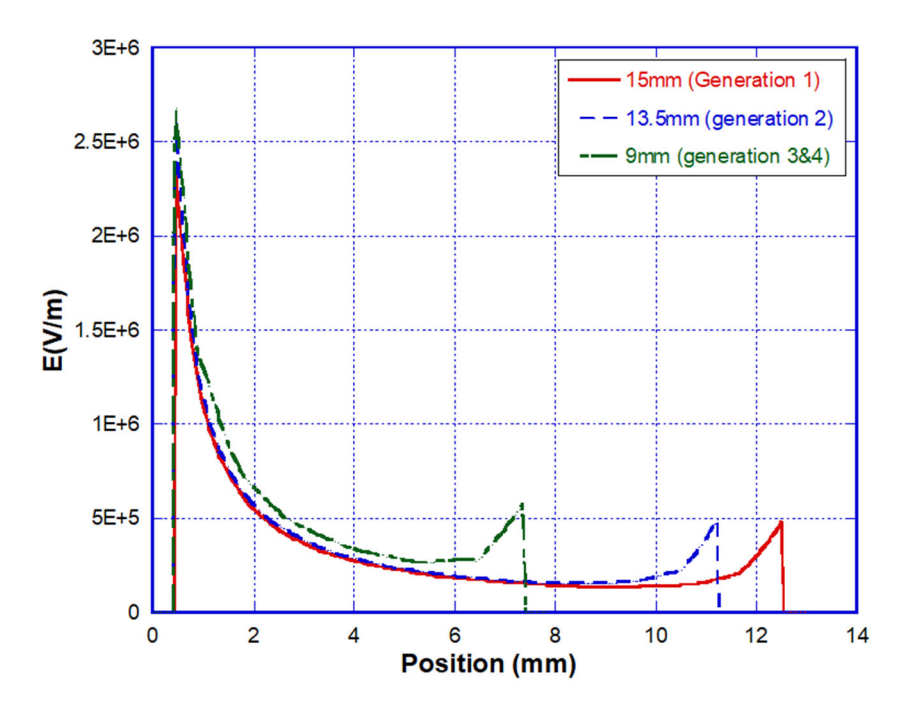


Figure 16: Electric field in radial direction of a hexagonal unit cells for all four generation desorbers.

4.2.2 Study on Electrical Waveforms

Experiment was conducted to determine the optimal electrical waveforms to drive the electrostatic desorber. A waveform generator was used to produces a variety of waveforms at a desired frequency. The electrical waveforms tested in the desorber are shown in Figure 17, which include Sine waves, Square waves, Triangular and, Rising waveforms. The test results are listed in Table 3. Initially, the microemulsion had a water concentration of 3.6497%. After applying the aforementioned electrical waveforms, the square waveform could regenerate the microemulsion with the least residual water concentration, as shown in Table 3. Further experiments were performed to determine the optimal frequency and amplitude (i.e., voltage) of the electrical waveforms. It was found that 4kV, 5-10kHz square waveform worked best for the electrostatic desorbers tested in the experiment.

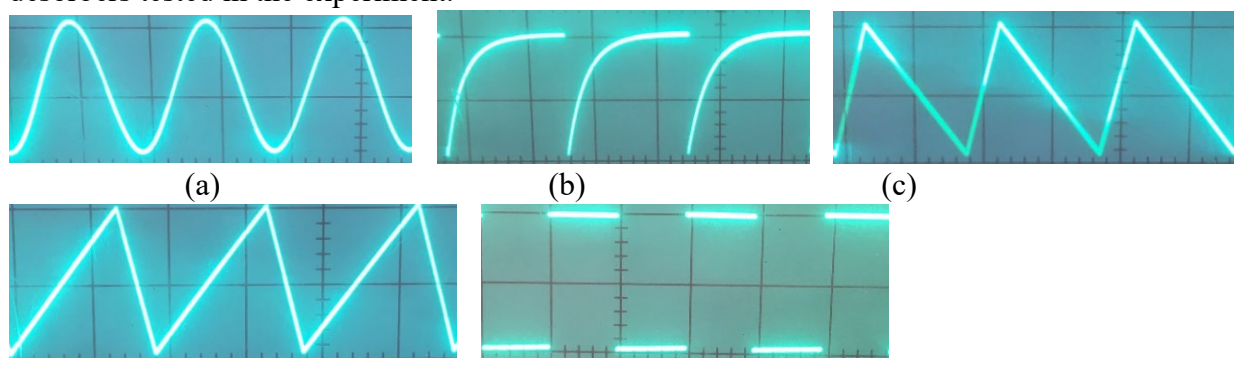


Figure 17: Electrical waveforms tested in the electrostatic desorber (a) Sine wave; (b) Rising wave; (c) Triangle wave-1:3; (d) Triangle wave-3-1; (e) Square wave

High Voltage Electrodes	Low Voltage Electrodes	Frequency	Initial water concentration wt%(H ₂ O)	Wave shape	Residual water in microemulsion wt%(H ₂ O)
				sine wave	2.5966%
				rising wave	2.7444%
4 kV	4 kV 0 V 10 kHz 3.6497% 1:3	10 kHz	3.6497%	triangle wave- 1:3	2.6447%
		triangle wave- 3:1	2.7056%		
				square wave	2.3641%

Table 3. Performance of different electrical waveforms

4.2.3 Assembly of Electrostatic Desorber

The design layout of the electrostatic desorber with the test flow loop is shown in Figure 18. This desorber system consisted of a desorber container with electrode array, an electric voltage supply unit, a flow loop equipped with heaters, temperature sensors and flow meters, and an oven that hosts the desorption container. This desorber system was manufactured and assembled, as shown in Figure 19.

The capacity of the microemulsion desorber could be calculated by the following equation, $Q = \frac{m*\Delta H_v}{t}$, where m is the mass of the separated water from the microemulsion, t is the desorption time, ΔH_v is the heat of vaporization of water (i.e., 2440J/g). The amount of the separated water could be determined from the water concentration change in the microemulsion before and after the electrostatic separation process. The capacity of the desorber with one separation flask was found to be about 260W. Two reaction flasks were connected in parallel to increase the capacity of the desorber, and its capacity was increased to about 520W.

Two approaches are recommended to further increase the capacity of the desorption system: 1) use a larger reaction flask in which electrode arrays could divide into small units. 2) connect several reaction flasks in parallel. Both approaches were found to be effective in increase the desorber capacity in out experiment.

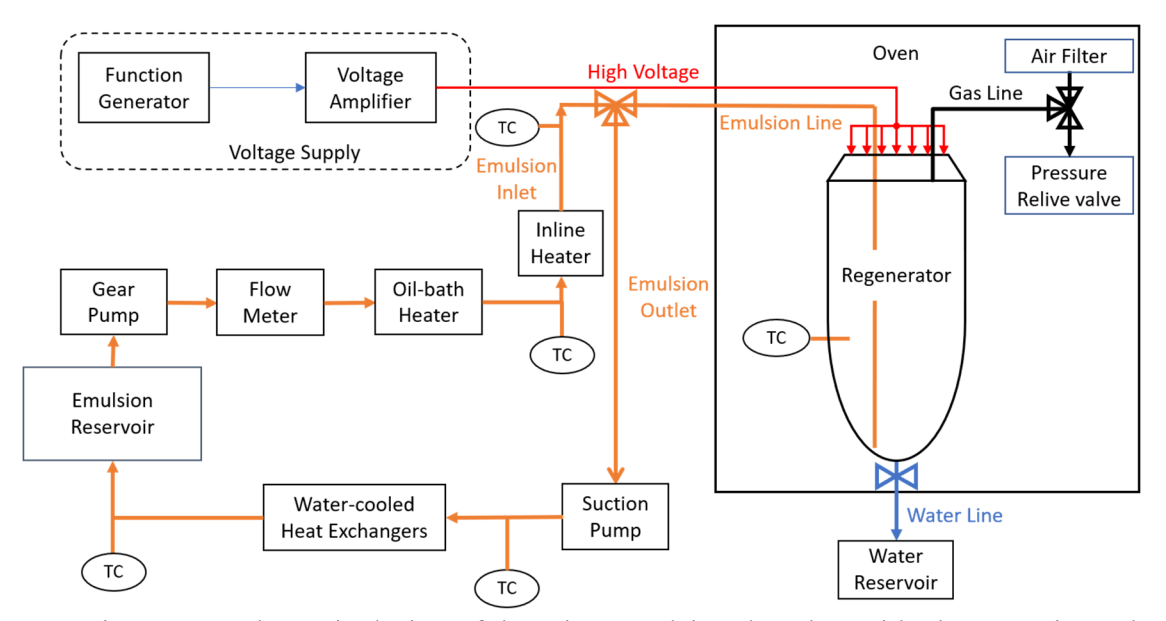


Figure 18: Schematic design of the microemulsion desorber with electrostatic coalescer.

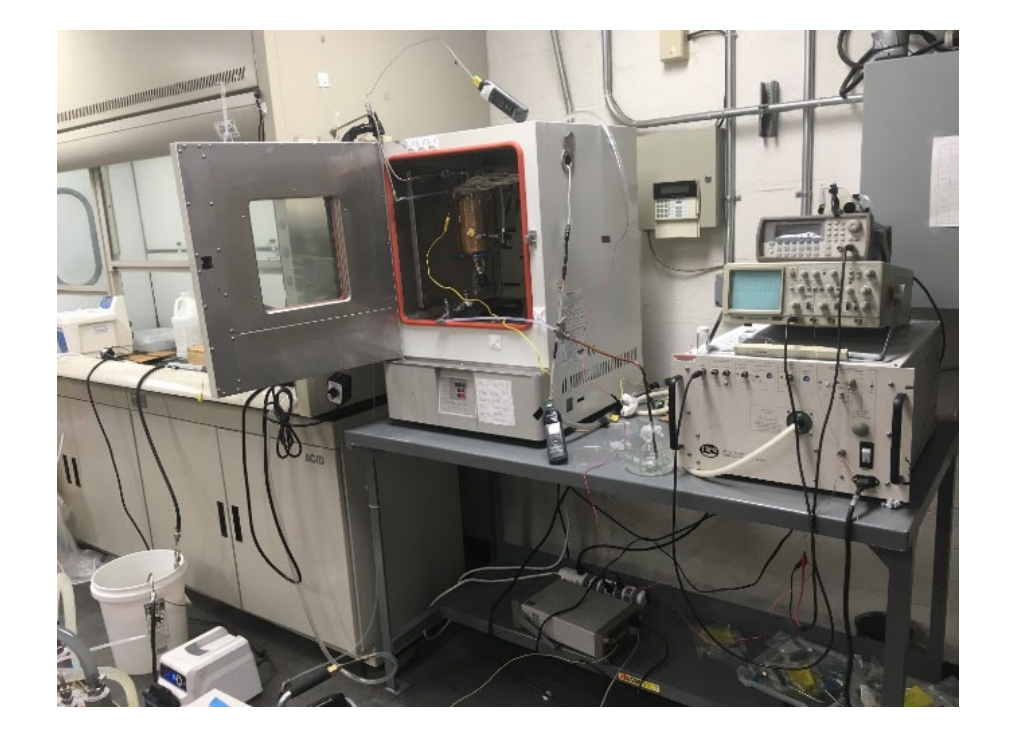


Figure 19: Photo of the microemulsion desorber with electrostatic coalescer

5. Development of Microemulsion Absorber with Atomizing Spray Nozzles

An absorber is a critical component in the microemulsion absorption chiller, in which water vapor is absorbed by the microemulsion absorbent. The diffusion coefficient of refrigerant water in the microemulsion absorbent was found to be $\sim 4.9 \times 10^{-11} m^2 s^{-1}$, about 30 times less than the value in lithium bromide/water.[3] An advanced absorption technology with atomizing spray nozzles was developed to improve the vapor absorption rate in the microemulsion. Modeling analysis were also conducted to understand how the microemulsion droplet size impacted the absorption rate.

5.1 Modeling On Absorption Process In Microemulsion Droplets

The absorption of water vapor into microemulsion droplets was determined by two steps: one was convective mass transfer outside the microemulsion droplet, and the other was water diffusion inside the microemulsion droplet. Two limiting cases were investigated: (a) absorption limited by the diffusion inside the droplet; (b) absorption limited by the diffusion outside the droplet

Case 1: absorption limited by diffusion inside the microemulsion droplet

In case I, the ratio of average water mass fraction to maximum possible water mass fraction in a microemulsion droplet can be calculated using the following formula,[15]

$$\frac{m_{\text{H}_2\text{O}}}{m_0} = \begin{cases} 6\sqrt{\frac{Fo_m}{\pi}} - 3Fo_m, & Fo_m < 0.2\\ 1 - \frac{6}{\pi^2} \exp(-\pi^2 Fo_m), & Fo_m \ge 0.2 \end{cases}$$
(10)

where $m_{\rm H_2O}$ is the average water mass fraction in a microemulsion droplet, and m_0 is the maximum possible water mass fraction in a microemulsion droplet. Fourier number Fo_m is defined as,

$$Fo_m = \frac{D_{\text{water}}t}{r^2} \tag{11}$$

where D_{water} is the diffusion coefficient of water in microemulsion which is about $4.9 \times 10^{-11} \,\text{m}^2/\text{s}$, t is diffusion time, and t is the radius of the microemulsion droplet.

Figure 20 shows the ratio of average water mass fraction to maximum possible water mass fraction in a microemulsion droplets as a function of absorption time for microemulsion droplet with different diameters (100-400 um). It can be seen that the water diffusion is faster for smaller droplets. The diffusion becomes slower with increasing absorption time. Figure 21 shows the ratio of average water mass fraction to maximum possible water mass fraction in a microemulsion droplet versus the droplet dimeter for different time durations (0.1 s, 0.5 s and 1 s). It can be seen that the diffusion rate exponentially decreases with the microemulsion droplet size.

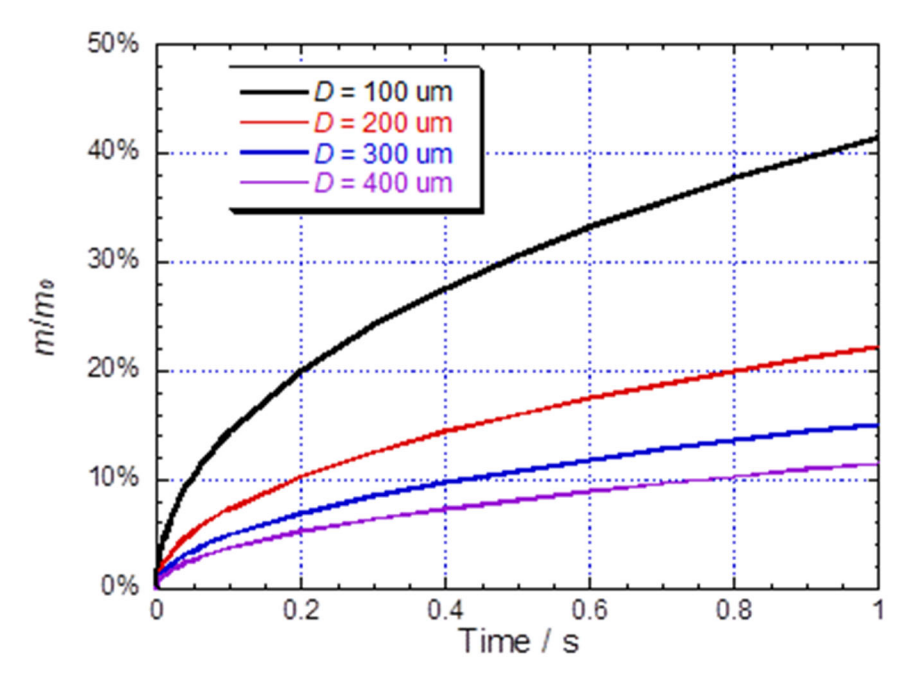


Figure 20: Ratio of average water mass fraction to maximum possible water mass fraction in a microemulsion droplet as a function of absorption time for microemulsion droplets with different diameters (100-400 um), for the limiting case when absorption is limited by the diffusion inside the droplet.

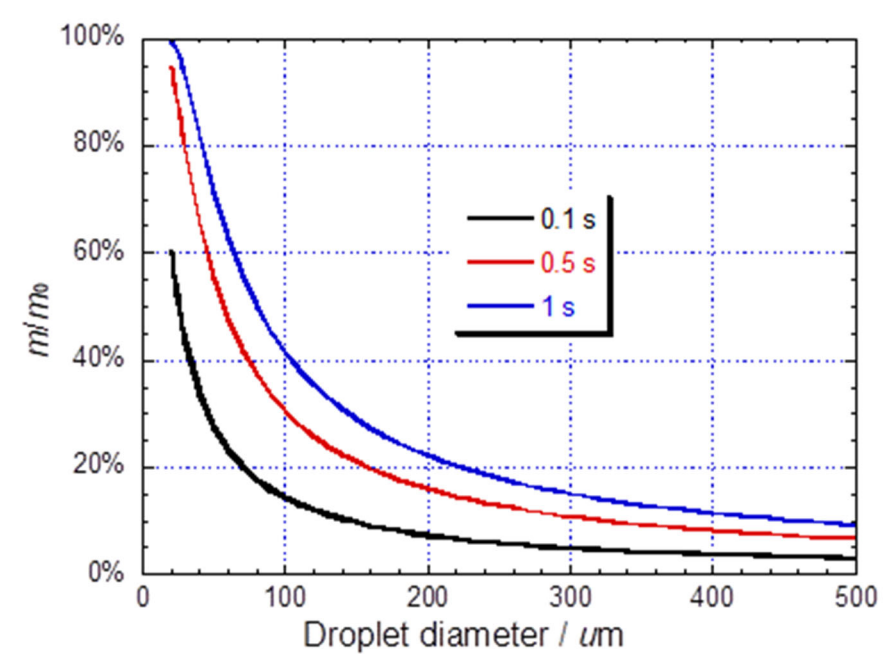


Figure 21. Ratio of average water mass fraction to maximum possible water mass fraction in a microemulsion droplet as a function of the droplet dimeter for different time durations (0.1 s, 0.5 s and 1 s), for the limiting case when absorption is limited by the diffusion inside the droplet.

Case 2: absorption limited by convective mass transfer outside the microemulsion droplet

In case 2, the mass conservation equation in a microemulsion droplet is given by,

$$h_{m} \cdot 4\pi r^{2} (0.95c_{H_{2}O}^{*} - c_{H_{2}O}^{I}) M_{H_{2}O} = \frac{d}{dt} \left(\frac{4}{3}\pi r^{3} \rho m_{H_{2}O} \right)$$
 (12)

where h_m is the convective mass transfer coefficient in m/s, $c_{\text{H}_2\text{O}}^*$ is the saturation water vapor concentration at 20 °C in mol/m³, $c_{\text{H}_2\text{O}}^{\text{I}}$ is the water vapor concentration at the gas-liquid boundary in mol/m³, and $M_{\text{H}_2\text{O}}$ is the molar mass of water. Using the ideal gas law, eq. (12) can be written as

$$h_{m} \cdot 4\pi r^{2} \left(\frac{0.95 p_{\text{H}_{2}\text{O}}^{*}}{RT} - \frac{p_{\text{H}_{2}\text{O}}^{\text{I}}}{RT}\right) M_{\text{H}_{2}\text{O}} = \frac{d}{dt} \left(\frac{4}{3}\pi r^{3} \rho m_{\text{H}_{2}\text{O}}\right)$$
(13)

Here $p_{\rm H_2O}^*$ is the saturation water vapor pressure at 20 °C in Pa, R is the gas constant in J/mol/K, T is temperature in K, $p_{\rm H_2O}^{\rm I}$ is the water vapor pressure at the gas-liquid boundary in Pa, $M_{\rm H_2O}$ is the molar mass of water in kg/mol. Eq. (13) can be further written as

$$h_{m} \cdot 4\pi r^{2} \frac{p_{H_{2}O}^{*}}{RT} (0.95 - RH) M_{H_{2}O} = \frac{d}{dt} \left(\frac{4}{3} \pi r^{3} \rho m_{H_{2}O} \right)$$
 (14)

Here RH is the relative humidity at the gas-liquid boundary. Rearranging eq. (14) gives

$$\frac{dm_{\rm H_2O}}{dt} + \frac{3h_{\rm m}M_{\rm H_2O}p_{\rm H_2O}^*}{r\rho RT}RH = 0.95 \times \frac{3h_{\rm m}M_{\rm H_2O}p_{\rm H_2O}^*}{r\rho RT}$$
(15)

Here RH is a function of $m_{\rm H_2O}$ which can be experimental measured for specific water concentrations in microemulsion. Hence, eq. (15) is an ordinary differential equation about $m_{\rm H_2O}$ and can be numerically solved.

Figure 22 shows the ratio of average water mass fraction to maximum possible water mass fraction in a microemulsion droplet as a function of absorption time for microemulsion droplets with different diameters (100-400 um). It can be seen that the diffusion rate increases with decreasing droplet diameter. The small microemulsion droplets get saturated within 1 second. By comparison of Figure 20 and Figure 22, it can be seen that the diffusion rate for the second limit case is much faster than that for the first limit case for the same droplet diameter. It is found experimentally that the water vapor absorption into microemulsion is very slow, which indicates that the diffusion process is mainly limited by the small water diffusion rate inside the microemulsion droplets.

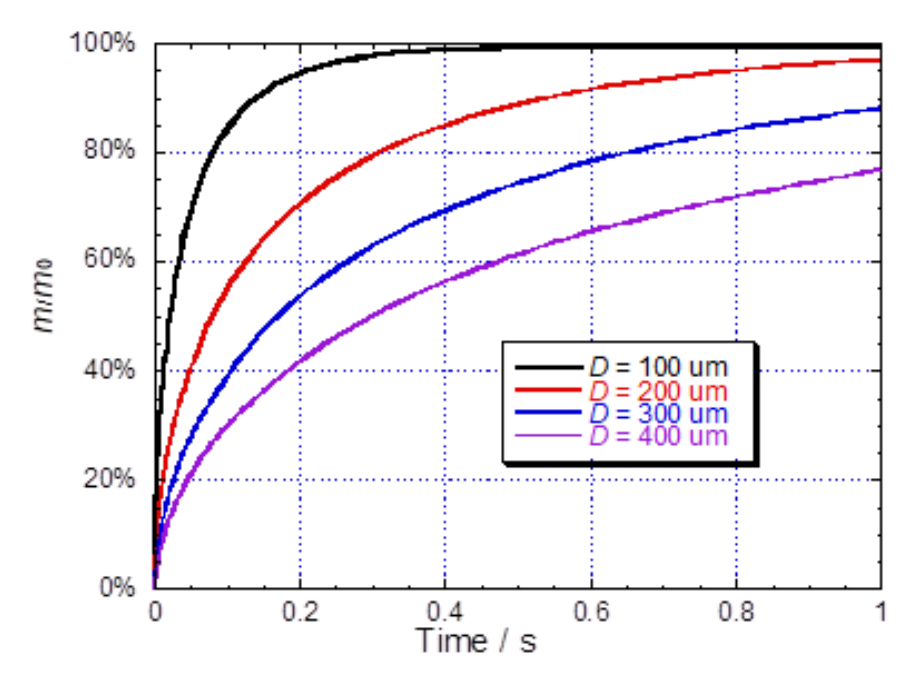


Figure 22. Ratio of average water mass fraction to maximum possible water mass fraction in a microemulsion droplet as a function of absorption time for microemulsion droplets with different diameters (100-400 um), for the second limiting case where vapor absorption is limited by convective mass transfer outside the microemulsion droplet.

5.2 Numeric Simulation on Absorption of Vapor in Microemulsion Droplet

To further investigate this absorption problem, a three-dimensional model was developed to simulate the transient diffusion process in the microemulsion droplet. Figure 23 is the comparison of simulation results and analytical results for the first limit case for a microemulsion droplet 300 microns in diameter. It is seen that when the moving velocity of the droplet is large and therefore the convective mass transfer coefficient is large, the simulation result is in well agreement with the result for the limit case 1. Figure 24 shows the boundary mass fraction of water in a microemulsion droplet 300 micron in diameter for 1 m/s and a very large velocity at which the droplet moves. It is seen that the boundary mass fraction of water goes up extremely fast and approaches a value equal to the water mass fraction corresponding to an *RH* of 95%. It is clear that the diffusion process inside the droplet limits the diffusion rate of water.

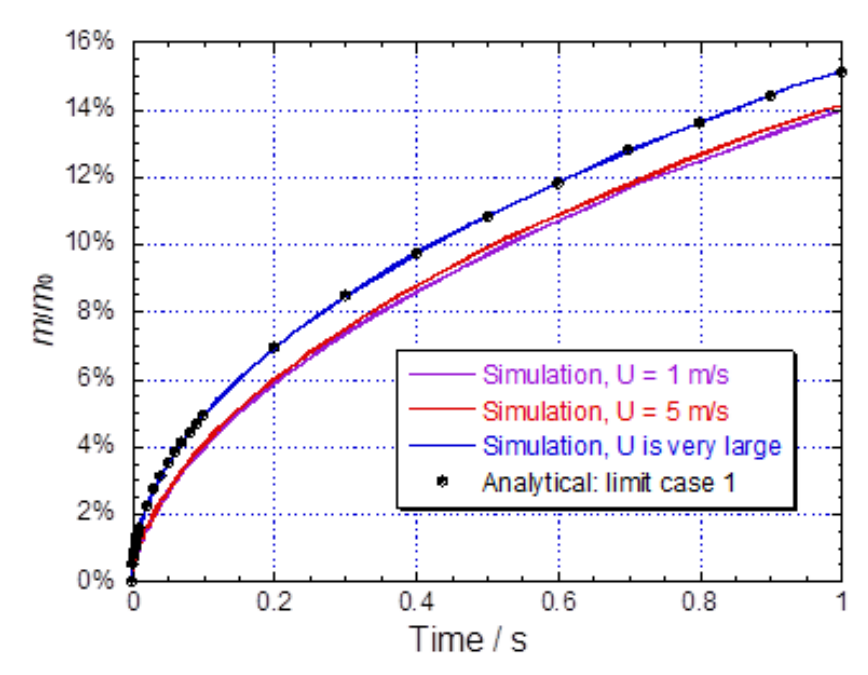


Figure 23: Ratio of average water mass fraction to maximum possible water mass fraction in a microemulsion droplet obtained from the analytical model (dots) and numeric simulation (lines).

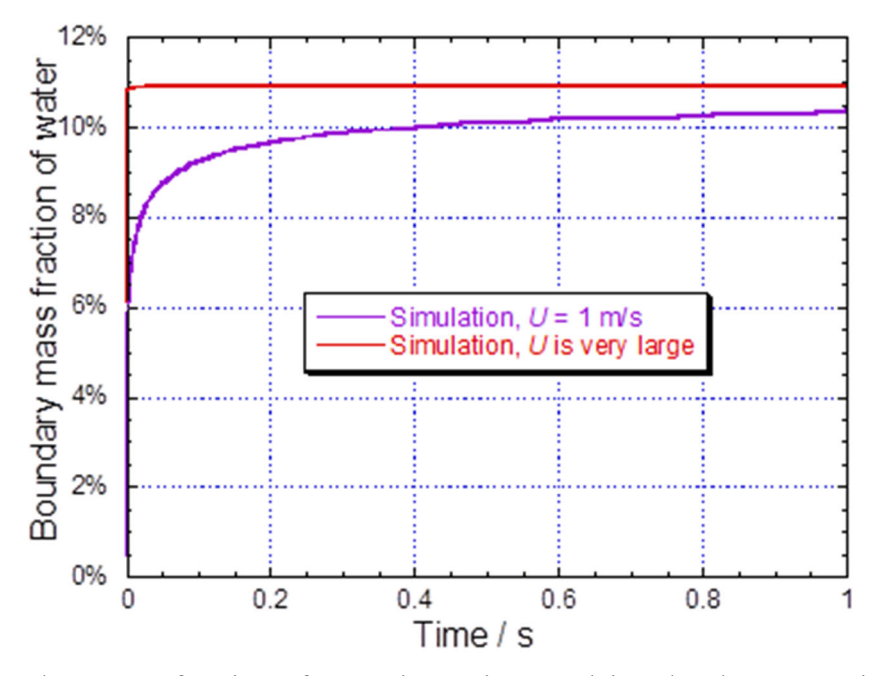


Figure 24: Boundary mass fraction of water in a microemulsion droplet 300um in diameter as a function of absorption time for different moving velocity U.

Numeric simulation was also to compare the absorption processes in both microemulsion droplets and thin films with same thickness/diameter. Figure 25 shows the distribution of the ratio of the water mass fraction to the maximum possible water mass fraction in a microemulsion droplet with *a diameter of* 100 um and 500um. It takes about 10 seconds for the 100um microemulsion

droplets to get saturated, while it takes much longer time for 500um droplets. This similar numeric simulation was conducted for the microemulsion thin films under the same absorption conditions.

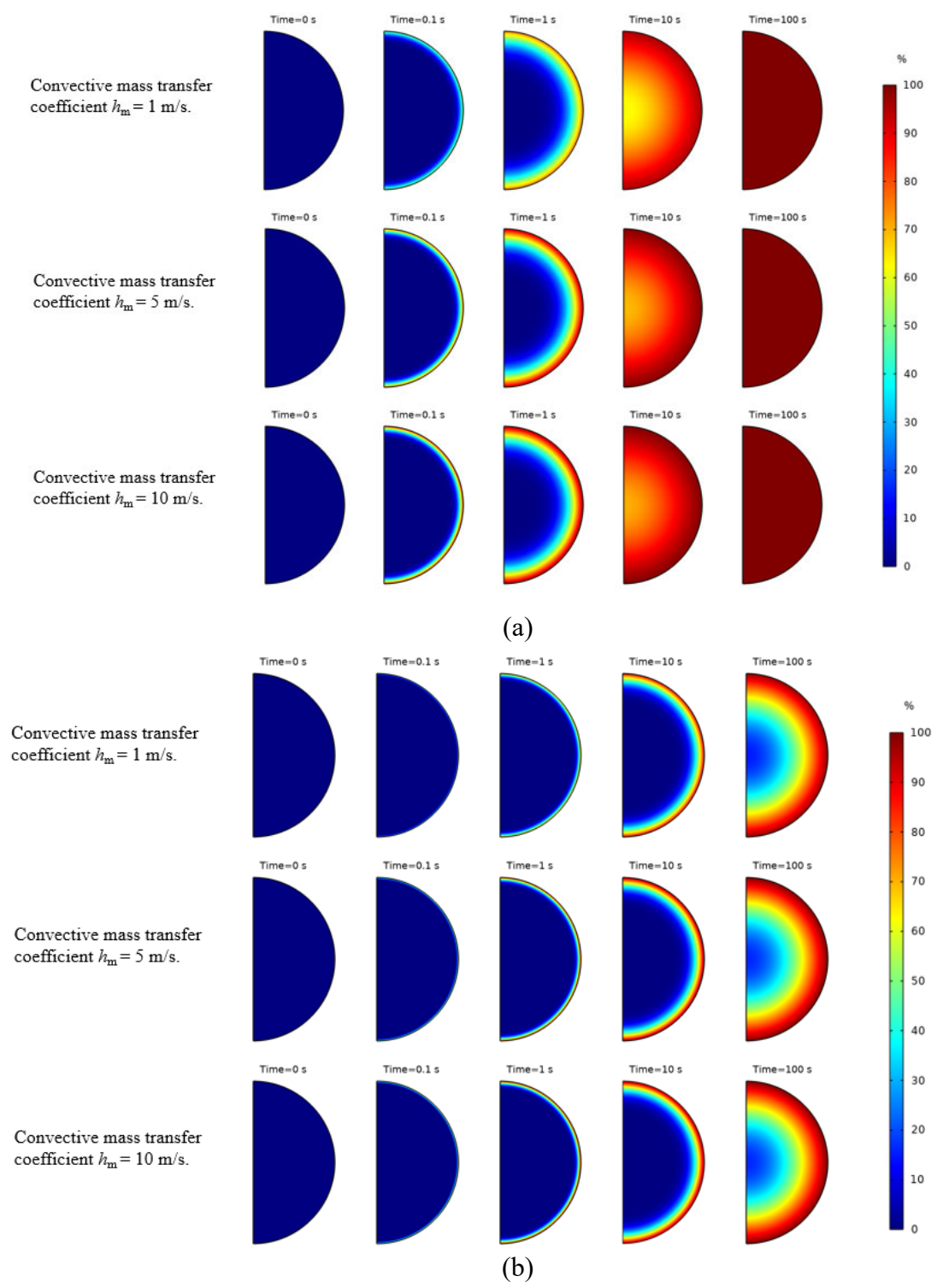


Figure 25: Contour of the ratio of average water mass fraction to maximum possible water mass fraction in a microemulsion droplet with a diameter of (a) 100um and (b) 500um, at different absorption time for different convective mass transfer coefficients.

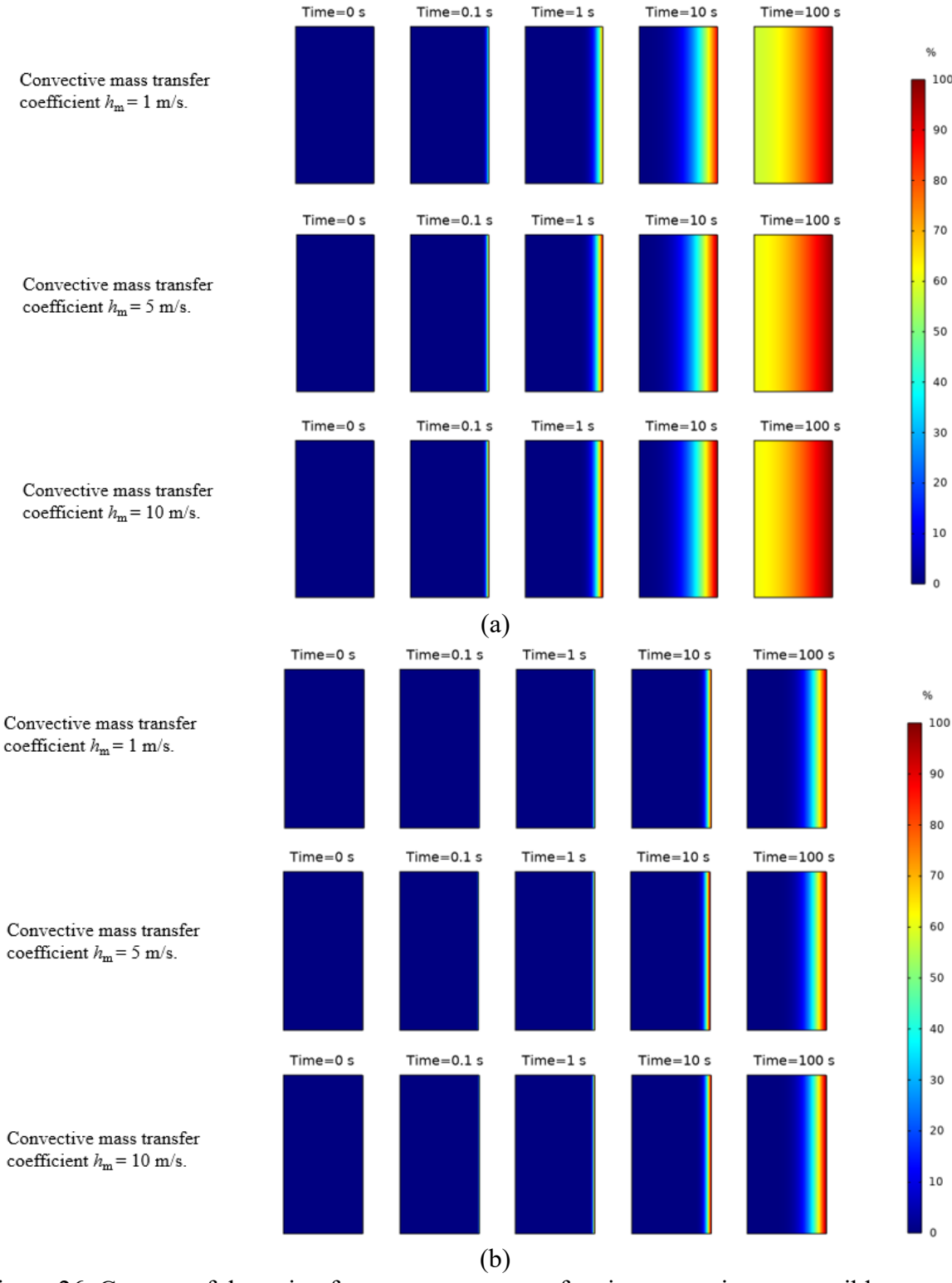


Figure 26: Contour of the ratio of average water mass fraction to maximum possible water mass fraction in a microemulsion thin film with a thickness of (a) 100um and (b) 500um, at different absorption time for different convective mass transfer coefficients.

Some important findings from the numeric simulation are below: 1) The change in convective mass transfer coefficient has little effect on the absorption rate. It is clear that the diffusion process inside the droplet limits the absorption rate of water. 2) Droplet size/film thickness is an important factor that affects the absorption rate. The droplet size need to be reduced to increase the absorption rate. 3) Droplets have higher surface to volume ratio than thin films, and therefore droplets are more efficient in the absorption process.

5.3 Experimental Results for Absorber

5.3.1 Atomization Techniques For Microemulsion

Two atomization techniques: ultrasonic atomizer and hydraulic spray nozzle, were tested in order to produce the microemulsion droplets. It was found that the ultrasonic atomizer didn't work when it was placed in the absorber in vacuum because of its thermal management issue. In comparison, the hydraulic spray nozzles are passive devices and capable generate fine microemulsion droplets in the absorber.

Figure 27 shows structure configuration of different hollow-cone nozzles. These hollow cone nozzles can be ordered according to the size of their generated droplets: hydraulic atomizing (fine spray) nozzles< Unijet nozzles < tangential whirl nozzles< spiral design nozzles. As shown in Figure 27(a), as liquid passes through slots in the core component of a hydraulic atomizing nozzle, it spins in a circle at a very high speed. The energy from the spinning action causes the liquid to break up into very small droplets.

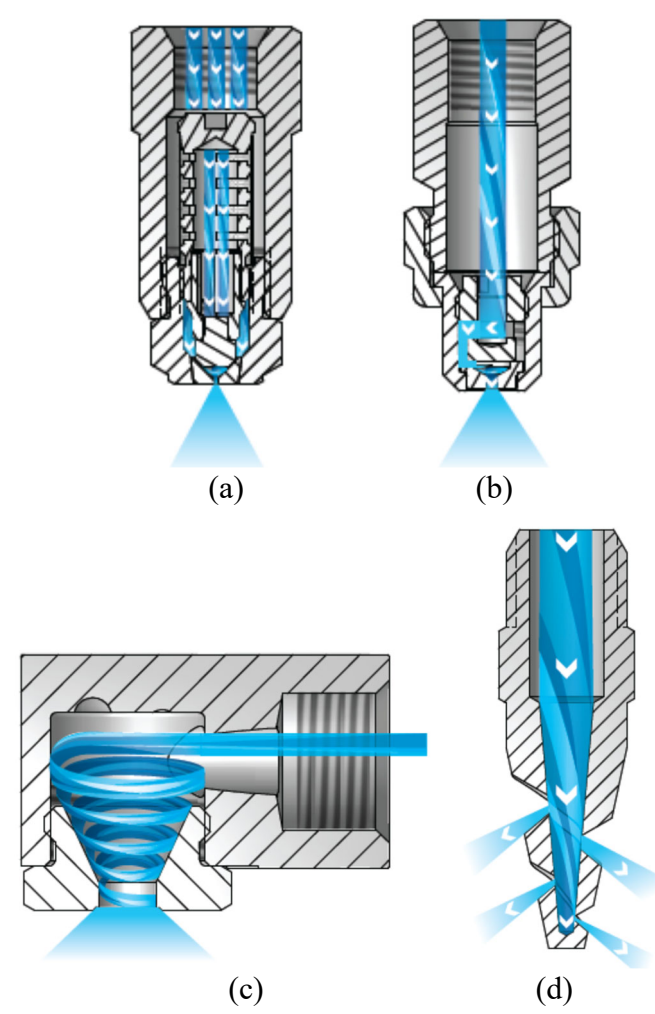


Figure 27: Structure of different hollow-cone nozzle design. (a) hydraulic atomizing nozzle; (b) Unijet nozzle; (c) tangential whirl nozzle; (d) spiral design nozzle. (Images from Spraying System Co)[16]

Many hydraulic nozzles have been tested to generate microemulsion droplets. Fine spray 1/4N-SS8 and Hollow cone D4-13-SS nozzles are best among them for our application. The performance data of these two nozzles are listed in Table 4. It can be seen these two nozzles have similar flow rate capacities at the same differential pressure.

Table 4: Performance Data of two nozzles from Spraying System Co.[16]

Nozzle type	Fluid	Flow rate capacity (ml/min)			Spray angle (°)	
Fine spray 1/4N-SS8		30 psi	40 psi	60 psi	40 psi	80 psi
	Water	435.3	504.7	618.3	85	89
Hollow cone D4-13-SS		416.4	454.2	530.0	79	83

5.3.2 Configuration of Integrated Absorber and Evaporator

Figure 28 shows the schematic design of the absorber and evaporator together with balance of system components. Figure 29 shows the absorber and evaporator system developed in this project. This system consists a microemulsion absorbent loop and a refrigerant water loop. The major components of the absorber include a steel vacuum chamber, an emulsion collection tank, spray nozzles, gear pumps, an emulsion reservoir, a pressure gauge, a heat exchanger, a water circulator, and temperature and humidity sensors. The microemulsion is pumped from a reservoir container to a heat exchanger and then to the spray nozzles. The temperature of the microemulsion is controlled by the water circulator through the heat-exchanger. The microemulsion is fed to the absorber where it absorbs water vapor. The weak microemulsion absorbent in the collection tank is pumped back to the reservoir through another gear pump.

The configuration of the evaporator is similar to that of the absorber. The major components of the evaporator include a steel vacuum chamber, a water collection tank, spray nozzles, gear pumps, a water reservoir, a pressure gauge, a heat exchanger, a water circulator, and temperature sensors. The refrigerant water is pumped from a reservoir container to a heat exchanger and then to the spray nozzles. The temperature of the water is controlled by the water circulator through the heat-exchanger. The water is fed to the evaporator where it evaporates and becomes cooled. The chilling water in the collection tank is pumped back to the reservoir through another gear pump. Both the absorber and evaporator are integrated inside one steel vacuum chamber.

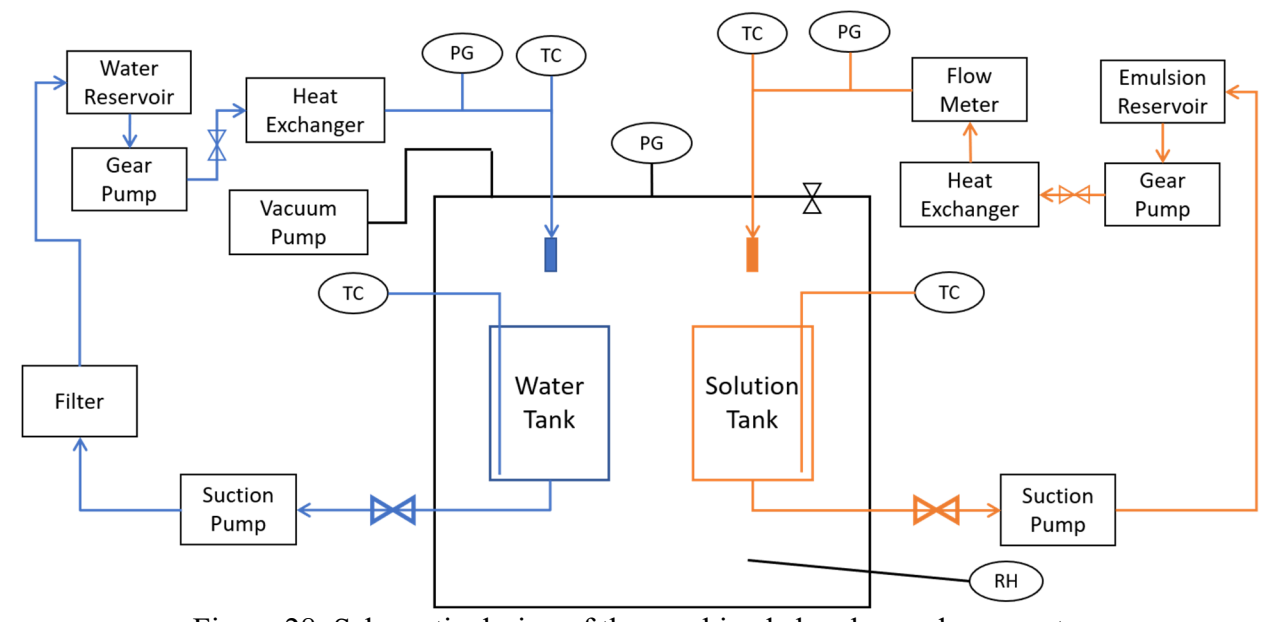
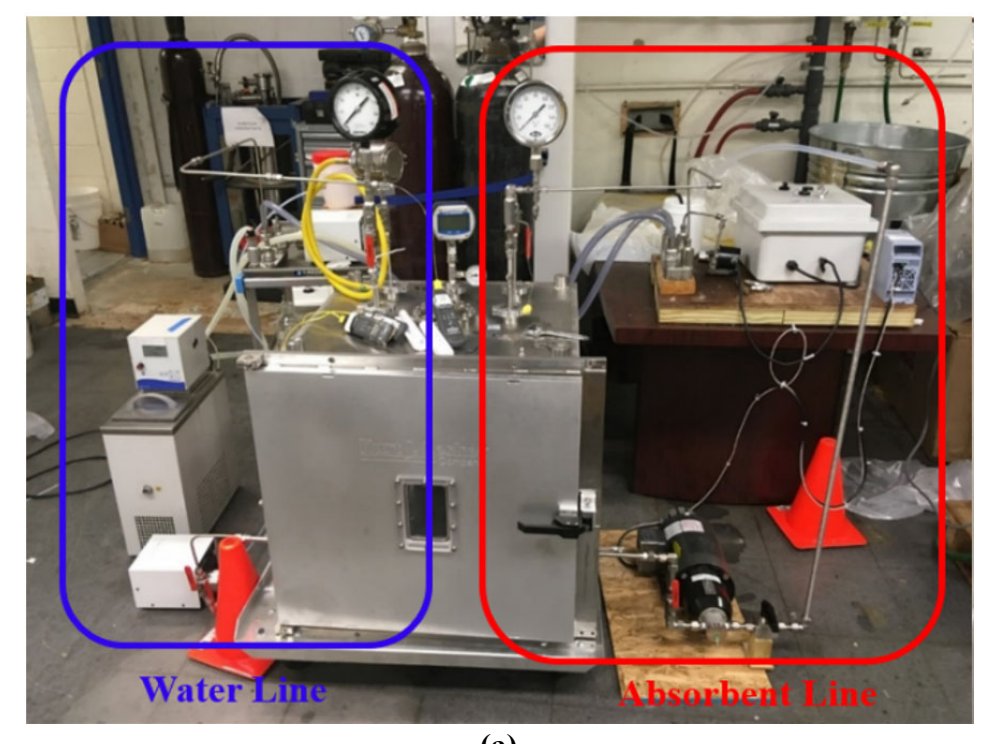


Figure 28: Schematic design of the combined absorber and evaporator.



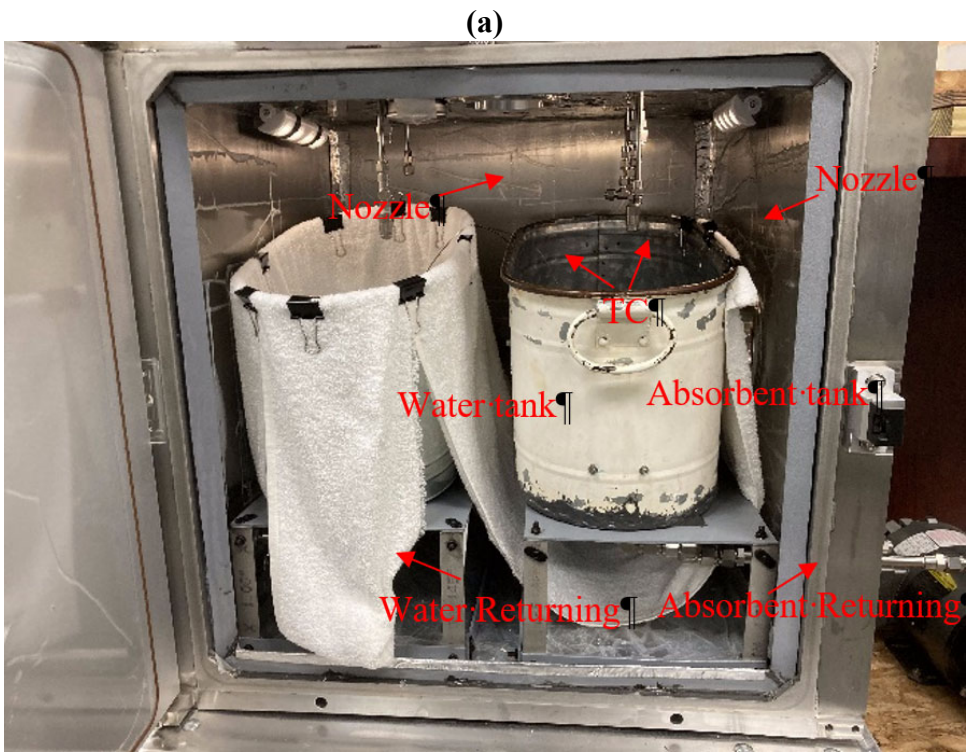


Figure 29: Picture of the combined absorber and evaporator. (a: outside the vacuum chamber; b: inside the vacuum chamber)

(b)

The cooling capacity of the microemulsion absorber can be calculated by the following equation, $Q_{cooling} = \frac{m*\Delta H_v}{t}$, where m is the mass of the absorbed water by the microemulsion, t is the absorption time, ΔH_v is the heat of vaporization of water (i.e., 2440J/g). The mass of the absorbed water m can be calculated from the water concentration change in the microemulsion before and after the absorption process. The capacity of the absorber with one spray nozzle was found to be about 177W. Two nozzles were connected in parallel to increase the capacity of the absorber, and its capacity was increased to about 240W. The capacity of the absorber could be further increased to 320 W when the flow rate of the microemulsion was increased from 1671 mL/min to 2182 mL/min

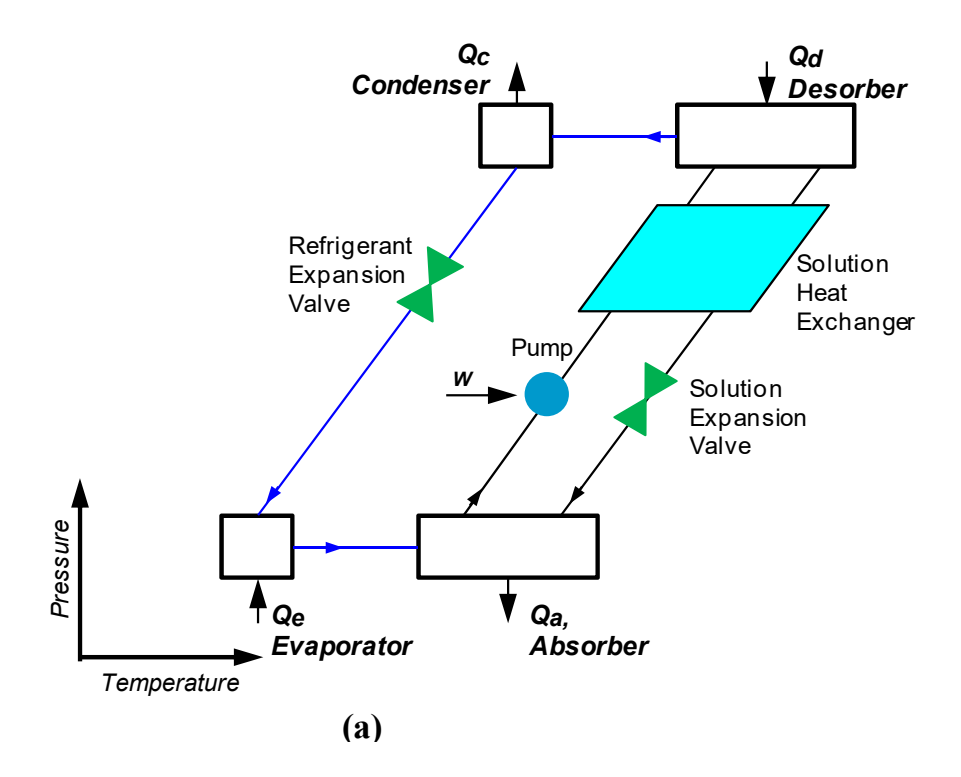
The use of two nozzles could increase the interface area between microemulsion and vapor, and therefor increased the cooling power. However there existed a significant spray overlap due to the limited space of the vacuum chamber, which affected the efficiency of the two nozzle system.

Two approaches are recommended to further increase the capacity of the desorption system: 1) a larger absorber chamber which can host more nozzles without overlapping. 2) smaller droplets generated by advanced atomization techniques. The current nozzles are designed and optimized for water, not for oil-based microemulsion.

6. Development of prototype microemulsion-based absorption chiller

6.1 Overall System Configuration

Figure 30a and b show the comparison between thermodynamic cycles of a conventional absorption chiller and the absorption chiller using microemulsion absorbents investigated in this project. As seen in Figure 30b, the microemulsion absorption chiller consists of three major components: absorber, desorber, and evaporator. The microemulsion thermodynamic cycle does not require a water condenser, since the refrigerant water can be separated as liquid without vaporization or boiling when sufficient heat is supplied to the desorber. The thermodynamic cycle of the microemulsion absorption chiller includes a solution loop and refrigerant loop. In the solution loop, the microemulsion solution circulates between the desorber and absorber. The microemulsion solution is pumped from the absorber, at low pressure, to the desorber, at higher pressure. In the absorber, the microemulsion absorbs water vapor from the evaporator. When heat is supplied to the microemulsion solution in the desorber, the refrigerant water is separated as a liquid without vaporization or boiling. Subsequently the regenerated microemulsion solution flows back to the absorber. The refrigerant loop of the absorption chiller is similar in function to the corresponding components in a vapor-compression cycle, except with no condenser, since the water is separated as a liquid from the solution in the desorber.



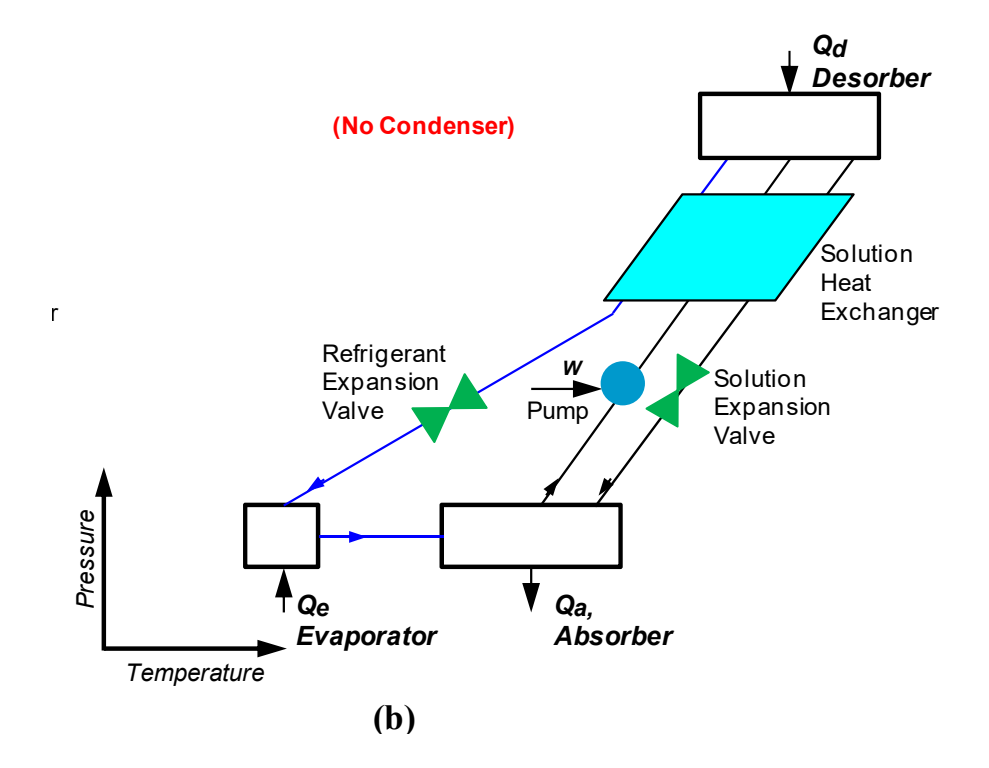


Figure 30: Schematic of thermodynamic cycle of (a) an absorption chiller using conventional absorbents and (b) the absorption chiller using microemulsion absorbents. In the system configuration in (b), the condenser is not needed.

6.2 Experimental Results for the Absorption Chiller

The schematic design of the microemulsion absorption chiller is shown in Figure 31. This system consists of an electrostatic desorber with two regenerator flasks connected in parallel, an absorber with two spray nozzles connected in parallel, an evaporator, a steel vacuum chamber that hosts both the absorber and evaporator, an oven that hosts two regenerator flasks, flow controls using 3-way valves, flow pumps, heat exchangers, flow meters, and temperature and pressure sensors.

In Figure 31, the orange line represents the microemulsion absorbent flow. The microemulsion absorbent solution circulates between the desorber and absorber. In the absorber, the microemulsion absorbs refrigerant water vapor and its water concentration increases. In the desorber, the refrigerant water is separated as a liquid and is drained out from the bottom of the regenerator flasks. Several 3-way valves are used to control the microemulsion flow between the desorber and absorber. The blue line in Figure 31 represents the refrigerant water flow between the desorber and evaporator. The prototype absorption chiller using the microemulsion as absorbent was manufactured, as shown in Figure 32.

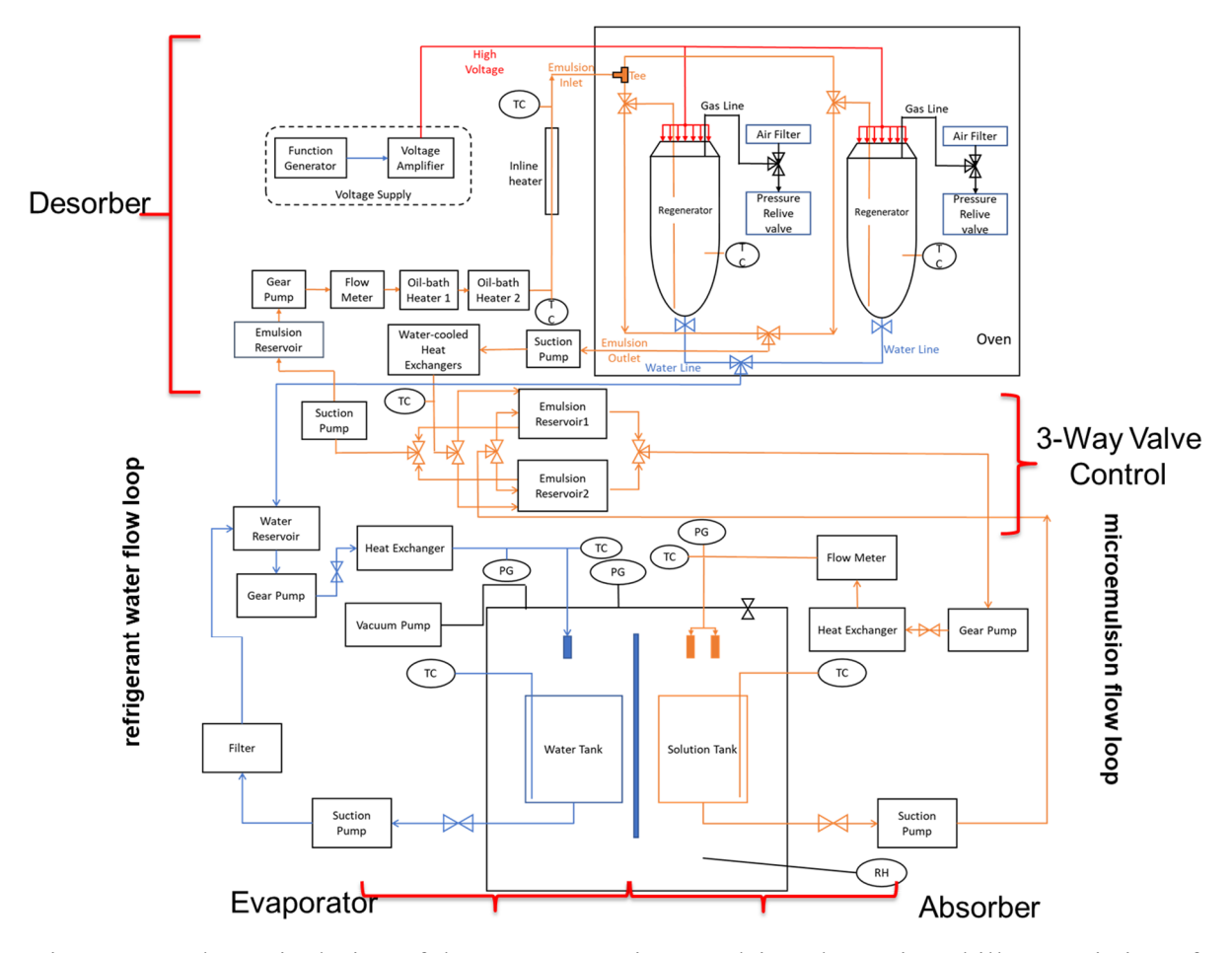


Figure 31: Schematic design of the prototype microemulsion absorption chiller consisting of a desorber, an absorber, an evaporator, and flow loops equipment with pumps, temperature sensors and flow meters.



Absorber & Evaporator

Figure 32: Picture of the prototype absorption chiller using the microemulsion as absorbent. It consists of three major components: desorber, absorber and evaporator.

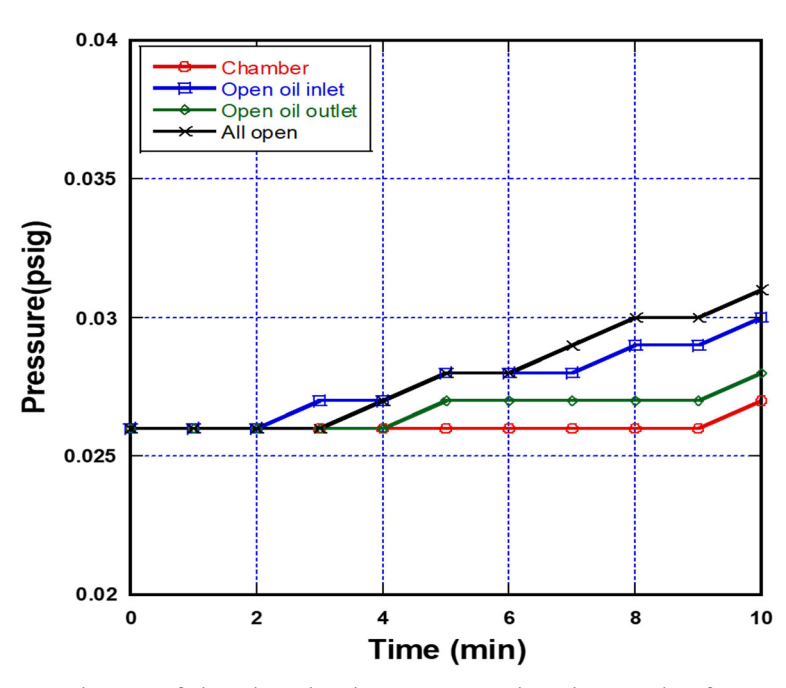


Figure 33: Leak test of the absorber/evaporator chamber under four conditions

The leak test of the absorber and evaporator chamber was conducted under four conditions in which the valves connected to the chamber were opened one by one. The results are shown in Figure 33. The leak rate was found to be less than 0.0005 psi/min, and the residual pressure inside was about 0.03psig, which is negligible compared to the water vapor pressure 0.41psig at 23 C (i.e., operation temperature of the evaporator).

The prototype microemulsion absorption chiller was operated on a continuous batch process. Each batch lasted for about 6 minutes, which was the time required to complete one desorption process. Between two batches, the microemulsion with high water content was pumped from the absorber to the desorber, while the regenerated microemulsion with low water content was pumped from the desorber to the absorber. Figure 34 shows the temperatures of the microemulsion solution (red line) and refrigerant water (blue line) in the absorber/evaporator chamber during the four batches process. The microemulsion temperature was kept around 25 C while the refrigerant water temperature was around 23.5 C. Figure 35 shows the total pressure of the absorber/evaporator chamber during the experiment.

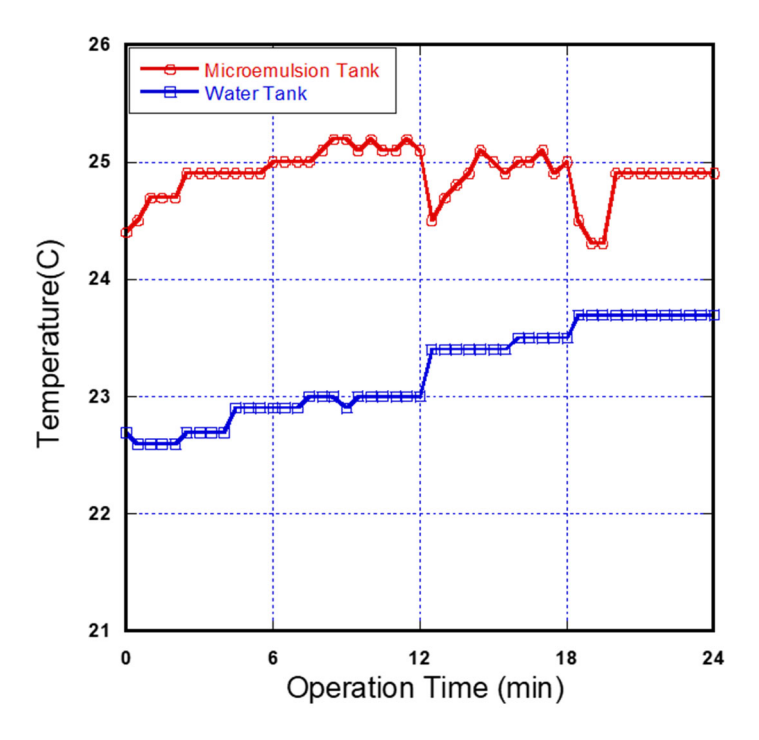


Figure 34: Temperature of microemulsion solution in the absorber (red line) and temperature of refrigerant water in the evaporator (blue line) during the experiment.

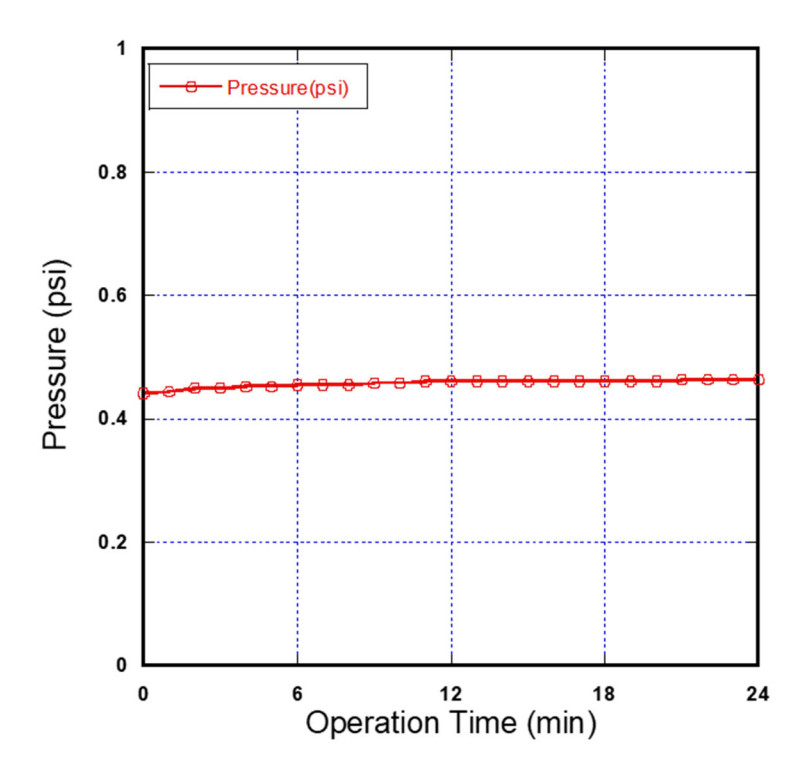


Figure 35: Pressure of the absorber/evaporator chamber during the experiment.

The water content of the microemulsion solution in the absorber was measured before and after each batch process, and the results are shown in Table 5. The cooling capacity of the microemulsion absorber can be calculated by the following equation, $Q_{cooling} = \frac{m*\Delta H_v}{t}$, where m is the mass of the absorbed water by the microemulsion, t is the absorption time, ΔH_v is the heat of vaporization of water (i.e., 2440J/g). The mass of the absorbed water m can be calculated from the water concentration change in the microemulsion before and after each batch process. The maximum possible capacity of this prototype absorption chiller was found to be about 258W, which did not include various heat losses to the chiller system.

Table 5: Water content in the microemulsion solution

Batch Number	1	2	3	4
Initial water content (wt. %)	3.03	3.05	3.24	3.21
Final water content (wt. %)	7.21	6.83	6.91	6.95

7. Conclusions and Future Research Recommendation

7.1 Conclusions of Experimental and Theoretical Work

An absorption chillers can be driven by low-grade heat and their refrigerants do not contribute to global warming and ozone depletion. The absorption chiller using the microemulsion as absorbent does not require a water condenser, and it may provide a way to improve the absorption chiller performance. Various technologies were explored to enhance the performance of the desorber and absorber components in the absorption chillers. A desorber with electrostatic coalescer was developed to separate quickly the refrigerant water from the microemulsion. The dielectrophoresis force exerted on the water droplets accelerated the droplet coalescence process significantly. It was found that the desorption time with the electrostatic filed could be reduced by more than 10 times compared to the desorption process without the electrostatic field. The strategy to scale up the electrostatic-coalescence desorber was developed by using electrode arrays to divide a large container into small units. An absorber was also developed in which the spray nozzles were used to produce fine microemulsion droplets. Different atomizing spray nozzles were tested for maximization of the absorption rate. The strategy to scale up the absorber capacity was also investigated. A prototype absorption chiller utilizing the microemulsion absorbents was manufactured and analyzed. The condenser, one of the major components in the traditional absorption chillers, was no longer needed in this chiller system. These research results demonstrated the feasibility and difficulties of developing a new generation of absorption chillers based on the microemulsions that have the potential to significantly improve the cooling performance.

7.2 Limitation of the Research and Future Research Recommendation

- 1) The cooling temperature, i.e., the temperature of the refrigerant water in the evaporator, in the prototype microemulsion-based absorption chiller is about 23 C. In comparison, the commercial single-effect LiBr-based absorption chillers can provide cooling below 10 C. Further research is needed to lower the cooling temperature of the microemulsion-based absorption chillers.
- 2) The cooling capacity of the microemulsion-based absorption chiller is limited by its absorber. This is probably due to the fact that the diffusion coefficient of refrigerant water in the microemulsion is about 30 times less than the value in lithium bromide/water. It was found that reducing the microemulsion droplet size, i.e., increasing the ratio of surface to volume, was an effective way to increase the absorption. Some commercial spray nozzles were capable of producing fine microemulsion droplets. But those spray nozzles were designed for water, not for oil-based microemulsion. As a future work, the optimization of spray nozzles for microemulsion droplets should be tackled.
- 3) To transition the developed technologies to market, competitive advantages need to be assessed and advertised to potential manufacturing partners. This includes understanding the interaction of players and stakeholders in the value chain, who these players/stakeholders, competitors, customers, end users are, how buying decisions are made, where the value (\$) is made, and how/where the technology can best be inserted.

7.3 Journal Publications and Conference Products

The journal publications and conference products associated with this award are listed below:

- 1) Bao Yang, Chaolun Zheng, and Hak Seung Lee, "Development of Novel Microemulsion Absorption Chillers", presented at the 6th ASME International Conference of Micro/Nanoscale Heat and Mass Transfer, July 8-10, 2019, Dalian, China.
- 2) Chaolun Zheng, Jian Zhou, Yong Pei, and Bao Yang, "Equilibrium Thermodynamic Properties of Aqueous Solutions of Ionic Liquid 1-Ethyl-3-Methylimidazolium Methanesulfonate [EMIM][MeSO3]", Scientific Reports, vol. 10, article number 3174 (2020). https://doi.org/10.1038/s41598-020-59702-z.
- 3) Chaolun Zheng, Ziyang Shen, Jian Zhou, Yong Pei, and Bao Yang, "Influences of the Anions on the Interaction Energy between Water and Ionic liquids", Chemical Engineering & Technology, vol. 45, pp.266-274, 2022. doi.org/10.1002/ceat.202100438

8. References:

- [1]. K. E. Herold, R. Radermacher and S. A. Klein, Absorption chillers and heat pumps. Boca Raton, FL: CRC Press, 1996.
- [2]. P. Srikhirin, S. Aphornratana and S. Chungpaibulpatana, "A review of absorptionrefrigeration technologies," Renewable & Sustainable Energy Reviews, vol. 5, pp. 343-372, 2001.
- [3]. V. Oberg and D. Goswami, "A Review of Liquid desiccant Cooling," Advances in Solar Energy, vol. 12, pp. 431-470, 1998.
- [4]. B. Yang, "Innovative, Microemulsion-Enabled Absorption/Adsorption Chiller and Heat Pump", U.S. Provisional Patent, 61/858,952, 2012.
- [5]. B. Yang and R. Radermacher, "Innovative, Microemulsion-enabled Water Capture and Recovery Technology", U.S. Provisional Patent, 61/987,280, 2014.
- [6]. B. Yang, R. Radermacher, F. Cao and B. Shi, "Application of Microemulsion-enabled Water Capture and Recovery Technology and Absorption/Adsorption Chiller in Power Plants", U.S. Provisional Patent, 61/867509, 2013.
- [7]. B. Yang and J. Xu, "Novel Working Paris for Absorption/Adsorption Refrigeration and Heat Pump", Invention Disclosure, PS-2010-101, 2010.
- [8]. Chromatography/Fourier transform infrared spectroscopy and its applications, by Robert White. ISBN 9780367450885, Published by CRC Press.
- [9]. "Near-Infrared Spectroscopy in Food Analysis". Encyclopedia of Analytical Chemistry. John Wiley & Sons. doi:10.1002/9780470027318.a1018. ISBN 9780470027318. Osborne BG (2006).
- [10]. How can I distinguish functional group region and fingerprint region in a infrared spectrum?: Socratic. (2015, January 23). Retrieved from https://socratic.org/questions/how-can-i-distinguish-functional-group-region-and-fingerprint-region-in-a-infrar.
- [11]. Mayerhöfer, Thomas Günter; Popp, Jürgen (2018). "Beer's law why absorbance depends (almost) linearly on concentration". ChemPhysChem. 20 (4): 511–515. doi:10.1002/cphc.201801073. PMID 30556240.
- [12]. Nishimura, A., Tatemichi, A., Miura, H., & Sakamoto, T. (1987). Life estimation for IC plastic packages under temperature cycling based on fracture mechanics. IEEE transactions on components, hybrids, and manufacturing technology, 10(4), 637-642.
- [13]. How Is Temperature Cycle Test Equivalent to Field Life? EESemi.com FAQ, https://www.eesemi.com/faq/faq-tc-life.htm.
- [14]. Gaur, K. (2005). A framework to assess portfolio credit risk using accelerated hazard rates. The George Washington University.
- [15]. Lavine, A. S., and T. L. Bergman. "Small and large time solutions for surface temperature, surface heat flux, and energy input in transient, one-dimensional conduction." Journal of heat transfer 130.10 (2008).
- [16]. https://www.spray.com/